7

Total Internal Reflection Fluorescence

Daniel Axelrod, Edward H. Hellen, and Robert M. Fulbright

7.1. Introduction

The distribution and dynamics of molecules at or near surfaces are central to numerous phenomena in biology: for example, binding to and triggering of cells by hormones, neurotransmitters, and antigens; the deposition of plasma proteins upon foreign surfaces, leading to thrombogenesis; electron transport in the mitochondrial membrane; cell adhesion to surfaces; enhancement of the reaction rate with membrane receptors by nonspecific adsorption and surface diffusion of ligand; and the dynamical arrangement of submembrane cytoskeletal structures involved in cell shape, motility, and mechanoelastic properties.

In most of these examples, certain functionally relevant molecules coexist in both a surface-associated and a nonassociated state. If such molecules are detected by a conventional fluorescence technique (such as epi-illumination in a microscope), the fluorescence from surface-associated molecules may be dwarfed by the fluorescence from nonassociated molecules in the adjacent detection volume. As an optical technique designed to overcome this problem, total internal reflection fluorescence (TIRF) allows selective excitation of just those fluorescent molecules in close ($\sim$100 nm) proximity to the surface. TIRF can be used quantitatively to measure concentrations of fluorophores as a function of distance from the substrate or to measure binding/unbinding equilibria and kinetic rates at a biological surface. As applied to biological cell cultures, TIRF allows selective visualization of cell/substrate contact regions, even in samples in which fluorescence elsewhere would otherwise obscure the fluorescent pattern in contact regions. TIRF can be used qualitatively to observe the position, extent, composition, and motion of these contact regions.

Daniel Axelrod, Edward H. Hellen, and Robert M. Fulbright • Department of Physics and Biophysics Research Division, University of Michigan, Ann Arbor, Michigan 48109.

Topics in Fluorescence Spectroscopy, Volume 3: Biochemical Applications, edited by Joseph R. Lakowicz. Plenum Press, New York, 1992.

TIRF is conceptually simple. An excitation light beam traveling in a solid (e.g., a glass coverslip or tissue culture plastic) is incident at a high angle θ upon the solid/liquid interface to which the cells adhere. That angle θ, measured from the normal, must be large enough for the beam to totally internally reflect rather than refract through the interface, a condition that occurs above some "critical angle." TIR generates a very thin (generally less than 200 nm) electromagnetic field in the liquid with the same frequency as the incident light, exponentially decaying in intensity with distance from the surface. The field is called the "evanescent wave" and is capable of exciting fluorophores near the surface while avoiding excitation of a possibly much larger number of fluorophores farther out in the liquid. In Section 7.2, the electromagnetic field which excites TIR fluorescence is discussed.

As an excitation system, TIRF does not specifically refer to the pattern, intensity, or lifetime of the fluorescence emitted from the near-surface molecules which become excited. However, these emission characteristics are somewhat different from those far from a surface, and some of these differences may become experimentally useful. In Section 7.3, the emission pattern of a fluorophore near a dielectric surface (particularly the interface of water with either bare glass or metal-coated glass) is discussed.

TIRF is easy to set up on a conventional upright or inverted microscope with a laser light source or, in a special configuration, with a conventional arc source. TIRF is completely compatible with standard epi-fluorescence, bright-field, dark-field, or phase contrast illumination so that these methods of illumination can be switched back and forth readily. Some practical optical arrangements for observing TIRF through a microscope are described in Section 7.4.

As a technique for selective surface illumination at liquid/solid interfaces, TIRF was first introduced by Hirschfeld[1] in 1965. Other important early applications were pioneered by Harrick and Loeb[2] in 1973 for detecting fluorescence from a surface coated with dansyl-labeled bovine serum allbumin, by Kronick and Little[3] in 1975 for measuring the equilibrium constant between soluble fluorescent-labeled antibodies and surface-immobilized antigens, and by Watkins and Robertson[4] in 1977 for measuring kinetics of protein adsorption following a concentration jump. Previous reviews[5–7] contain additional references to some important early work. Section 7.5 presents a literature review of recent work.

7.2. Theory of TIR Excitation

7.2.1. Single Interface

When a light beam propagating through a transparent medium 3 of high index of refraction (e.g., glass) encounters an interface with medium 1 of lower

index of refraction (e.g., water), it undergoes total internal reflection for incidence angles (measured from the normal to the interface) greater than the "critical angle." The critical angle θ_c for TIR is given by

$$\theta_c = \sin^{-1}(n_1/n_3) = \sin^{-1} n \tag{7.1}$$

where n_1 and n_3 are the refractive indices of the liquid and the solid, respectively, and $n = n_1/n_3$ where $n < 1$ for TIR to occur. For incidence angle $\theta < \theta_c$, much of the light propagates through the interface with a refraction angle (also measured from the normal) given by Snell's law. (Some of the incident light internally reflects back into the solid.) For $\theta > \theta_c$, all of the light reflects back into the solid. However, even with TIR, some of the incident energy penetrates through the interface and propagates parallel to the surface in the plane of incidence. The field in the liquid, called the "evanescent field" (or "wave"), is capable of exciting fluorescent molecules that might be present near the surface.

For a finite-width beam, the evanescent wave can be pictured as the beam's partial emergence from the solid into the liquid, travel for some finite distance along the surface, and then reentrance into the solid. The distance of propagation along the surface is measurable for a finite-width beam and is called the Goos–Hanchen shift.

For an infinitely wide beam (i.e., a beam width many times the wavelength of the light, which is a very good approximation for our purposes), the intensity of the evanescent wave (measured in units of energy per unit area per second) exponentially decays with perpendicular distance z from the interface:

$$I(z) = I(0)e^{-z/d} \tag{7.2}$$

where

$$d = \frac{\lambda_0}{4\pi}(n_3^2 \sin^2\theta - n_1^2)^{-1/2} \tag{7.3}$$

with λ_0 the wavelength of the incident light in vacuum. Depth d is independent of the polarization of the incident light and decreases with increasing θ. Except for $\theta \to \theta_c$ (where $d \to \infty$), d is on the order of λ_0 or smaller.

A physical picture of refraction at an interface shows TIR to be part of a continuum, rather than a sudden new phenomenon appearing at $\theta = \theta_c$. For small θ, the light waves in the liquid are sinusoidal, with a certain characteristic period noted as one moves normally away from the surface. As θ approaches θ_c, that period becomes longer as the refracted rays propagate increasingly parallel to the surface. At exactly $\theta = \theta_c$, that period is infinite, as the wave fronts of the refracted light are normal to the surface. This situation

corresponds to $d=\infty$. As θ increases beyond θ_c, the period becomes mathematically imaginary; physically, this corresponds to the exponential decay of Eq. (7.2).

The factor $I(0)$ in Eq. (7.2) is a function of θ and the polarization of the incident light; these features are discussed shortly. However, we first examine the remarkable amplitude, polarization, and phase behaviors of the electric fields [from which $I(0)$ is derived] and the magnetic fields of the TIR evanescent wave. The field components are listed below, with incident electric field amplitudes $A_{p,s}$ and phase factors relative to those of the incident **E** field's phase at $z=0$. (The coordinate system is chosen such that the x–z plane is the plane of incidence. Incident polarizations p and s are parallel and perpendicular to the plane of incidence, respectively.)

$$E_x=\frac{(2\cos\theta)(\sin^2\theta-n^2)^{1/2}}{(n^4\cos^2\theta+\sin^2\theta-n^2)}A_p e^{-i(\delta_p+\pi/2)} \tag{7.4}$$

$$E_y=\frac{2\cos\theta}{(1-n^2)^{1/2}}A_s e^{-i\delta_s} \tag{7.5}$$

$$E_z=\frac{2\cos\theta\sin\theta}{(n^4\cos^2\theta+\sin^2\theta-n^2)^{1/2}}A_p e^{-i(\varphi_p+\pi/2)} \tag{7.6}$$

where

$$\delta_p\equiv\tan^{-1}\left[\frac{(\sin^2\theta-n^2)^{1/2}}{n^2\cos\theta}\right] \tag{7.7}$$

$$\delta_s\equiv\tan^{-1}\left[\frac{(\sin^2\theta-n^2)^{1/2}}{\cos\theta}\right] \tag{7.8}$$

Fields polarized parallel (p) or perpendicular (s) to the plane of incidence are given by

$$\mathbf{E}_p=E_x\hat{x}+E_z\hat{z}\qquad \mathbf{E}_s=E_y\hat{y} \tag{7.9}$$

where $\hat{x}$, $\hat{y}$, and $\hat{z}$ are unit vectors. For p-polarized fields,

$$\mathbf{E}_p=E_p(0)\exp(-z/2d)(\alpha_x\hat{x}+\alpha_z\hat{z}) \tag{7.10}$$

where

$$E_p(0)=A_p\frac{(2\cos\theta)(2\sin^2\theta-n^2)^{1/2}}{n^2\cos\theta+i(\sin^2\theta-n^2)^{1/2}} \tag{7.11}$$

and

$$\alpha_x=-i\left(\frac{\sin^2\theta-n^2}{2\sin^2\theta-n^2}\right)^{1/2}\qquad \alpha_z=\frac{\sin\theta}{(2\sin^2\theta-n^2)^{1/2}} \tag{7.12}$$

For s-polarized fields,

$$\mathbf{E}_s=E_s(0)\exp(-z/2d)\,\hat{y} \tag{7.13}$$

where

$$E_s(0)=A_s\frac{2\cos\theta}{\cos\theta+i(\sin^2\theta-n^2)^{1/2}} \tag{7.14}$$

Note that the evanescent field is purely transverse to the propagation direction ($+x$) only for the s polarization. The p-polarized field $\mathbf{E}_p$ "cartwheels" along the surface with a spatial period of $\lambda_0/(n_3\sin\theta)$ as shown schematically in Figure 7.1. The nonzero longitudinal component E_x distinguishes an evanescent field from freely propagating subcritical refracted light, which has no longitudinal component. As one might expect, E_x approaches zero as the incidence angle is reduced from the supercritical range back toward the critical angle.

For a finite-width incident beam, the incidence angle dependence of the phase factors δ_p and δ_s gives rise to the measurable longitudinal shift of the beam, known as the Goos–Hanchen shift. This shift ranges from a fraction of a wavelength at $\theta=90°$ to infinite at $\theta=\theta_c$, which of course corresponds to the refracted beam skimming along the interface. A finite incidence beam can be expressed as a weighted integral over infinite plane waves approaching at a range of incidence angles; each plane wave at each angle gives rise to its own exponentially decaying evanescent field of infinite lateral extent. The x–y intensity profile of the evanescent field for the finite beam can then be calculated by the weighted integral of these plane-wave-generated evanescent fields over the range of incident plane-wave angles. For a TIR Gaussian laser beam focused with a typically narrow angle of convergence, the evanescent

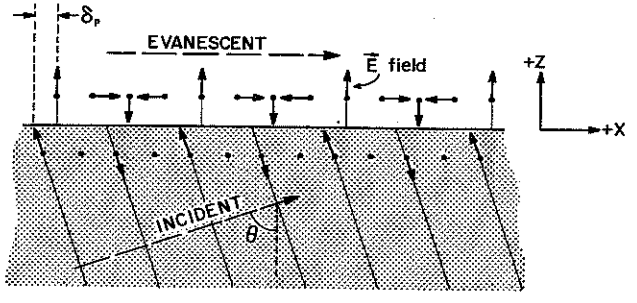

Figure 7.1. Electric field vectors of incident and evanescent light for the p-polarization, showing the phase lag δ_p and the elliptical polarization of the evanescent field in the plane of propagation. Both the incident and evanescent field vectors, shown here below and above the interface for pictorial clarity, refer to the $z=0$ position.

illumination is approximately an elliptical Gaussian profile, and the polarization and penetration depth are approximately equal to those of a single infinite plane wave.[8]

For absorbers with magnetic dipole transitions, the evanescent magnetic field **H** leads to absorption of electromagnetic energy. Assuming equal magnetic permeabilities at both sides of the interface, the components of the evanescent field **H** at $z=0$ are

$$H_x = \frac{(2\cos\theta)(\sin^2\theta - n^2)^{1/2}}{(1-n^2)^{1/2}} A_s e^{-i(\delta_s - \pi)} \tag{7.15}$$

$$H_y = \frac{2n^2\cos\theta}{(n^4\cos^2\theta + \sin^2\theta - n^2)^{1/2}} A_p e^{-i(\delta_p - \pi/2)} \tag{7.16}$$

$$H_z = \frac{2\cos\theta\sin\theta}{(1-n^2)^{1/2}} A_s e^{-i\delta_s} \tag{7.17}$$

The average energy flux in the evanescent wave is given by the real part of the Poynting vector $\mathbf{S} = (c/4\pi)\mathbf{E}\times\mathbf{H}^*$. However, the probability of absorption of energy per unit time from the evanescent wave by an electric dipole-allowed transition of moment $\boldsymbol{\mu}_a$ in a fluorophore is proportional to $|\boldsymbol{\mu}_a\cdot\mathbf{E}|^2$. Note that $\mathrm{Re}\,\mathbf{S}$ and $|\boldsymbol{\mu}_a\cdot\mathbf{E}|^2$ are not proportional to each other: they have a different dependence on θ.

Given randomly oriented dipoles, the absorption probability rate is proportional to the "intensity" $I_{p,s} \equiv |\mathbf{E}_{p,s}|^2$. At $z=0$, the evanescent intensities are

$$I_x(0) = |A_p|^2 \frac{(4\cos^2\theta)(\sin^2\theta - n^2)}{n^4\cos^2\theta + \sin^2\theta - n^2} \tag{7.18}$$

$$I_z(0) = |A_p|^2 \frac{4\cos^2\theta\sin^2\theta}{n^4\cos^2\theta + \sin^2\theta - n^2} \tag{7.19}$$

which gives, from $I_p = I_x + I_z$,

$$I_p(0) = |A_p|^2 \frac{(4\cos^2\theta)(2\sin^2\theta - n^2)}{n^4\cos^2\theta + \sin^2\theta - n^2} \tag{7.20}$$

Also,

$$I_s(0) = I_y(0) = |A_s|^2 \frac{4\cos^2\theta}{1-n^2} \tag{7.21}$$

Intensities $I_{p,s}(0)$ are plotted versus θ in Figure 7.2a, assuming the incident intensities in the glass, $|A_{s,p}|^2$, are set equal to unity. The plots can be

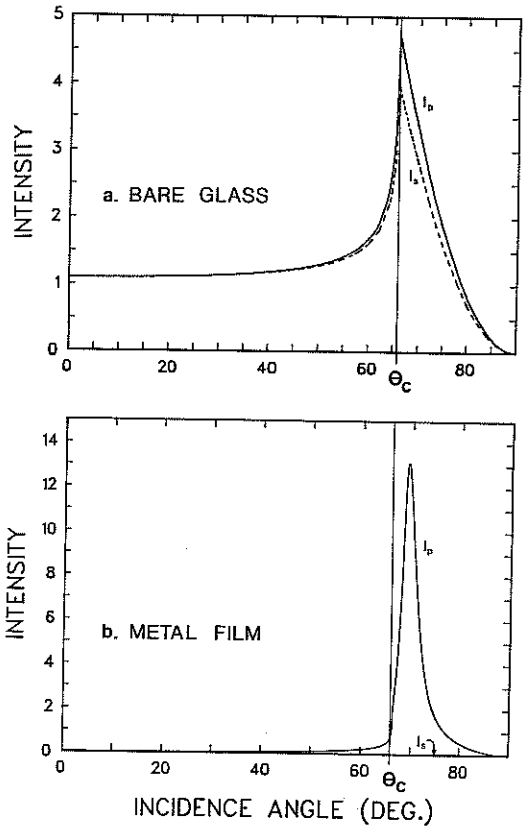

Figure 7.2. Intensity $I_p(0)$ (——) and $I_s(0)$ (– – –) versus incidence angle θ at (a) a bare fused-silica/water interface and (b) a 20-nm aluminum film-coated fused-silica/water interface. Intensity $I_s(0)$ for the aluminum film case is essentially zero. Refractive indices $n_3 = 1.46$ and $n_1 = 1.33$ are assumed, corresponding to $\theta_c = 65.7°$. Note the difference in ordinate scales (always set for $A_{p,s}^2 = 1$) between the bare glass and metal film case.

extended without breaks to the subcritical angle range (based on calculations with Fresnel coefficients), again illustrating the continuity of the transition to TIR. The evanescent intensity approaches zero as $\theta \to 90°$. On the other hand, for supercritical angles within ten degrees of θ_c, the evanescent intensity is as great as or greater than the incident light intensity.

7.2.2. Intermediate Layer

In actual experiments in biophysics, the interface may not be a simple interface between two media, but rather a stratified multilayer system. One example is the case of a biological membrane or lipid bilayer interposed between glass and aqueous media. Another example is a thin metal film coating, which quenches fluorescence within the first ~10 nm of the surface

(see Section 7.3). We discuss first qualitatively, then quantitatively, the TIR evanescent wave in a three-layer system in which incident light travels from medium 3 (refractive index n_3) through the intermediate layer (n_2) toward medium 1 (n_1).

Qualitatively, several features can be noted:

1. Insertion of an intermediate layer never thwarts TIR, regardless of the intermediate layer's refractive index, n_2. The only question is whether TIR takes place at the n_3:n_2 interface or the n_2:n_1 interface. Since the intermediate layer is likely to be very thin (no deeper than several tens of nanometers) in many applications, precisely which interface supports TIR is not important for qualitative studies.
2. Regardless of n_2 and the thickness of the intermediate layer, the evanescent wave's profile in medium 1 will be exponential with a characteristic decay distance given by Eq. (7.3). However, the overall distance of penetration of the field measured from the surface of medium 3 is affected by the intermediate layer.
3. Irregularities in the intermediate layer can cause scattering of incident light, which then propagates in all directions in medium 1. This subject has been treated theoretically.[9] Experimentally, scattering appears not to be a problem on samples even as inhomogeneous as biological cells. Direct viewing of incident light scattered by a cell surface lying between the glass substrate and an aqueous medium confirms that scattering is many orders of magnitude dimmer than the incident or evanescent intensity and should thereby excite a correspondingly dim contribution to the fluorescence.

To handle the three-layer problem quantitatively, we write the $z=0$ electric field components in terms of complex three-layer Fresnel coefficients:

$$E_x = -A_p \alpha_{13} T_p \tag{7.22}$$

$$E_y = A_s T_s \tag{7.23}$$

$$E_z = A_p (\varepsilon_3/\varepsilon_1)^{1/2} \sin\theta T_p \tag{7.24}$$

Parameters ε_i ($\equiv n_i^2$) are the dielectric constants of the respective media (which may be complex for light-absorbing materials). Parameters $T_{p,s}$ are the Fresnel coefficients for transmission through a stratified three-medium system with the beam incident from the medium 3 side and an intermediate medium 2 of thickness δ[10]:

$$T_{p,s} = \frac{t_{32}^{p,s} t_{21}^{p,s} e^{ik_1 \delta \alpha_{23}}}{1 + r_{32}^{p,s} r_{21}^{p,s} e^{2ik_1 \delta \alpha_{23}}} \tag{7.25}$$

where the t_{ij} and r_{ij} are the transmission and reflection coefficients for p- and s-polarized light for a single interface. They are listed here for convenience:

$$r_{ij}^p = \frac{\varepsilon_j \alpha_{i3} - \varepsilon_i \alpha_{j3}}{\varepsilon_j \alpha_{i3} + \varepsilon_i \alpha_{j3}} \qquad r_{ij}^s = \frac{\alpha_{i3} - \alpha_{j3}}{\alpha_{i3} + \alpha_{j3}} \tag{7.26}$$

$$t_{ij}^p = \frac{2(\varepsilon_i \varepsilon_j)^{1/2} \alpha_{i3}}{\varepsilon_j \alpha_{i3} + \varepsilon_i \alpha_{j3}} \qquad t_{ij}^s = \frac{2\alpha_{i3}}{\alpha_{i3} + \alpha_{j3}} \tag{7.27}$$

where

$$\alpha_{ij} \equiv \left(\frac{\varepsilon_i}{\varepsilon_1} - \frac{\varepsilon_j}{\varepsilon_1} \sin^2\theta \right)^{1/2} \tag{7.28}$$

and $k_1 \equiv (\omega/c)\varepsilon_1^{1/2}$, where ω is the excitation light angular frequency. Note that α_{ij} and $T_{p,s}$ can be complex. As expected, Eqs. (7.22)–(7.24) reduce to Eqs. (7.4)–(7.6) for $\varepsilon_2 = \varepsilon_3$. [Note that Eq. (7.26) corrects misprints in Eqs. (18) and (20) in Reference 6.]

The three-layered interface gives rise to evanescent intensities as follows:

$$I_p = |A_p|^2 |T_p|^2 \left(2\frac{\varepsilon_3}{\varepsilon_1} \sin^2\theta - 1 \right) e^{-z/d} \tag{7.29}$$

$$I_s = |A_s|^2 |T_s|^2 e^{-z/d} \tag{7.30}$$

I_p and I_s at $z=0$ are affected by n_2. If the intermediate layer is a thin ($\sim$20 nm) film of metal, the effect is dramatic (Figure 7.2b). A metal has a dielectric constant consisting of a negative real part and a positive imaginary part (for aluminum, $\varepsilon_2 = -32.5 + 8.4i$ at $\lambda_0 = 520$ nm). The s-polarized evanescent intensity $I_s(0)$ becomes negligibly small. However, the p-polarized behavior is quite interesting. At a certain angle of incidence θ_p, the denominator of t_{21}^p becomes quite small (due to the oppositely signed real parts of ε_2 and ε_1). At that incidence angle, the p-polarized evanescent intensity becomes an order of magnitude brighter than the incident light at the peak. This resonance-like effect is due to excitation of a surface plasmon mode at the metal/water interface. The peak is at the "surface plasmon angle," due to a resonant excitation of electron oscillations at the metal/water interface.[11–13] For an aluminum film at a glass/water interface, θ_p is greater than the critical angle θ_c for TIR. The intensity enhancement is rather remarkable since a 20-nm-thick metal film is almost opaque to the eye.

There are some potentially useful experimental consequences of TIR excitation through a thin metal film coated on glass. As discussed in Section 5.3, fluorescence from molecules less than 10 nm from the metal is strongly quenched. However, TIR can still be used to selectively excite fluorophores in the 10- to 200-nm distance range from metal-film-coated glass. Also, a

light beam incident upon a 20-nm-thick Al film from the glass side at a glass/aluminum film/water interface evidently does not have to be collimated to produce TIR. Those rays that are incident at the surface plasmon angle will create a strong evanescent wave; those rays that are too low or high in incidence angle will create a negligible field in the water. This phenomenon may ease the practical requirement for a collimated incident beam in TIR. Lastly, the metal film leads to a highly polarized evanescent wave (provided $A_p \neq 0$), regardless of the purity of the incident polarization.

7.3. Emission by Fluorophores near a Surface

Although the probability of absorption of TIR evanescent energy by a fluorophore of given orientation decreases exponentially with distance z from a dielectric surface, the intensity of the fluorescence actually viewed by a detector varies with z in a much more complicated fashion. Both the angular pattern of the emitted radiation and the fluorescent lifetime are altered as a function of z by the proximity of the surface.

These effects are not limited to fluorophores excited by TIR, although TIR excitation is necessarily near a surface. The discussion in this section is of relevance to any mode of excitation of surface-proximal fluorescence. In many of the experiments involving fluorescence in cell biology, the fluorophores are located near a surface. Usually, this surface is an aqueous buffer/glass or plastic interface upon which cells grow. Occasionally, the interface may have a thin coating on it, such as a synthetic polymer, a metal, or a lipid bilayer.

Various aspects of fluorophore emission at surfaces have been investigated, particularly within the past two decades. For nondissipative surfaces (e.g., bare glass), the lifetime[14] and the inversely related total radiated power[15] for a single emission dipole, modeled as a continuous classical oscillator, have been calculated as functions of orientation and distance from the surface. The radiated intensity emitted from a continuous dipole oscillator has been calculated as a function of observation angle, dipole orientation, and distance.[16–21]

For metal surfaces, most theoretical attention has been devoted to the dramatic decrease in lifetime and concomitant decrease in total radiated power near metal blocks, films, or microscopic islands.[12, 22–26] Several optical phenomena occur, each being important at a particular range of distances of the fluorophore from the surface. At distances comparable with or longer than visible wavelengths ($z > 500$ nm), the interference between the propagating (far-field) emitted light and its reflection dominates.[24, 25] At intermediate ranges (10 nm $< z <$ 500 nm), the evanescent near field of the dipole transfers some energy into propagating surface plasmons and into heat by way of the

local resistivity of the metal (i.e., electron scattering).[12, 13, 22, 27–29] At very close ranges ($z < 10$ nm), energy transfer into electron–hole pairs may become significant,[30, 31] and at atomic scale distances ($z < 0.25$ nm), nonhomogeneous local field effects become important.[32]

We present here a condensed explanation and summary of the effects. A complete discussion can be found in a paper by Hellen and Axelrod[33] which directly calculates the amount of emission light gathered by a finite-aperture objective from a surface-proximal fluorophore under steady illumination. The effects referred to here are not "quantum-chemical," that is, effects upon the orbitals or states of the fluorophore in the presence of any static fields associated with the surface. Rather, the effects are "classical-optical," that is, effects upon the electromagnetic field generated by a classical oscillating dipole in the presence of an interface between any media with dissimilar refractive indices. Of course, both types of effects may be present simultaneously in a given system. However, the quantum-chemical effects vary with the detailed chemistry of each system, whereas the classical-optical effects are more universal. Occasionally, a change in the emission properties of a fluorophore at a surface may be attributed to the former when in fact the latter are responsible.

This chapter deals only with the classical-optical effects. It emphasizes the emission properties as they might be observed through a microscope, with particular attention to the bare-glass/water and metal-film-coated glass/water interfaces. The results suggest some practical experiments that take advantage of the special optical effects at surfaces. These experiments include deducing the relative concentration of fluorophore as a function of distance from the surface, quenching unwanted "background" fluorescence from fluorophores nonspecifically adsorbed to a substrate, and optimizing collection of fluorescence by a microscope objective.

7.3.1. Description of the Model

Surface optical effects can be calculated at various levels of approximation. The simplest (and least accurate) approach is to model the fluorophore as an oscillating electric dipole of fixed amplitude generating only rays of propagating light (the "far field"). The rays (which are actually symbols for propagating plane waves) interact with the surface according to Snell's law and the law of reflection. Their uniformly spaced wave fronts (within each uniform refractive index medium) extend as semi-infinite planes. This approach considers the interference between such rays of propagating light directly emitted from the dipole and light rays reflecting off the interface. The results are valid only for distances z from the surface of greater than the wavelength of the light (~ 500 nm).

A better approximation must consider the so-called "near field." The mathematical form of a dipole radiation pattern cannot be expressed simply as a superposition of plane waves/rays propagating in different directions with direction-dependent amplitudes. Rather, it is necessary to suppose that some of the wave fronts do not extend infinitely far from the dipole but instead exponentially decay. A whole set of such exponentially decaying fields exists with a continuous range of decay constants. When a fluorophore (say, in water) is near a higher refractive index surface (say, glass), each of these exponentially decaying near-field components can interact with the surface and ultimately some become propagating waves in the glass at their own unique angles θ (with respect to the normal). Angle θ is always greater than the critical angle θ_c for total internal reflection. This conversion of exponentially decaying waves from the near field of the dipole in water into supercritical angle propagating waves in the glass can be significant for fluorophores within about one wavelength of the surface. At a metal surface, consideration of the near field is even more important, because the metal converts the electromagnetic energy into heat.

Another feature of the simplest model that needs modification is the assumption of a fixed dipole amplitude. Because of the efficient capture of nonpropagating near fields by a surface, a fixed-amplitude dipole emits more power, the closer it moves to a surface. However, in steady-state fluorescence, the emitted power can only be as large as the (constant) absorbed power (or less, if the intrinsic quantum yield of the isolated fluorophore is less than 100%). Therefore, the fluorophore must be modeled as a constant-*power* (and variable-*amplitude*) dipole. Many of the earlier theoretical references listed above deal only with constant-amplitude dipoles, so their results must be considered to be an approximation.

The two above features which modify the simplest theory extend the range of distances z between the fluorophore and the surface over which the results remain valid, from a minimum of several hundred nanometers without the modifications to less than ten nanometers with them. Those two features are incorporated into the results displayed here. Other refinements, not included here, involve consideration of energy transfer to electron–hole pairs (for metals only at $z < 10$ nm) and nonhomogeneous atomic field effects ($z < 0.25$ nm). We first assume that the intrinsic quantum yield is 100%; then we will modify that assumption.

7.3.2. Mathematical and Physical Basis

The model here consists of a medium 3 (refractive index n_3; e.g., glass), a sandwiched layer of thickness t (n_2; e.g., polymer, metal, lipid, or more of

medium 3), and a medium 1 (n_1; e.g., water). The $z = 0$ origin is at the $n_1 : n_2$ interface, and the dipole resides in medium 1 at $z \geqslant 0$.

In general, an electric field $\mathbf{E}'(\mathbf{r})$ emitted from an isolated, fixed-amplitude dipole (i.e., no surfaces nearby) can be expanded as an integral over plane waves (with sinusoidal time dependence suppressed) as follows:

$$\mathbf{E}'(\mathbf{r}) = \int d\mathbf{k} \exp(i\mathbf{k} \cdot \mathbf{r})\, \mathbf{E}'(\mathbf{k}) \tag{7.31}$$

where wave vector $\mathbf{k} = k_x \hat{x} + k_y \hat{y} + k_z \hat{z}$, and the integration extends over all $\mathbf{k}$, subject only to the restriction that the frequency of the light, ω, remain fixed. Emission field $\mathbf{E}'$ is primed to distinguish it from the excitation field $\mathbf{E}$, which is unprimed and discussed in Section 7.2. Vector $\mathbf{r}$ extends from the origin at the $n_1 : n_2$ interface to the point at which $\mathbf{E}'$ is observed. $\mathbf{E}'(\mathbf{k})$ can be determined directly via Maxwell's equations, or from the known form of dipole radiation $\mathbf{E}'(\mathbf{r})$ via Eq. (7.31). Since the magnitude of $\mathbf{k}$ is

$$|\mathbf{k}| = (k_x^2 + k_y^2 + k_z^2)^{1/2} = \omega n_1 / c \tag{7.32}$$

the integration in Eq. (7.31) requires only that $|\mathbf{k}|$ be held fixed. Propagating (sinusoidal) waves are described by k_x^2, k_y^2, and k_z^2, all positive. However, if we allow $(k_x^2 + k_y^2) > |\mathbf{k}|^2$, then $k_z^2 < 0$. Those "plane waves" have an imaginary k_z and correspond to exponentially decaying waves in either direction along the z-axis starting from the position of the dipole. This set of plane waves is the dipole's "near field." The amplitude and phase of each wave $\exp(i\mathbf{k} \cdot \mathbf{r})$, whether propagating or exponentially decaying, is given by $\mathbf{E}'(\mathbf{k})$.

The near-field wave fronts can be chosen to be parallel to the z-axis, exponentially decaying in amplitude in either direction along the z-axis starting from the dipole position and traveling radially outward parallel to the x–y plane. The apparent wavelength of each exponentially decaying wave is shorter than that of the propagating waves, corresponding to the large radial k-vector amplitude given by $k_r = (k_x^2 + k_y^2)^{1/2}$.

The electric field $\mathbf{E}_1'(\mathbf{r})$ observed at point $\mathbf{r}$ in medium 1 is then the superposition of the direct field [calculated from Eq. (7.31) for waves traveling away from the surface in the $+z$ direction] and plane reflected waves (calculated as described above), integrated over all allowed $\mathbf{k}$ vectors. The electric field $\mathbf{E}_3'(\mathbf{r})$ observed in medium 3 is an integral of the plane refracted waves, also integrated over all allowed $\mathbf{k}$. Note that Snell's law demands that the spacing between successive wave fronts as projected on a dielectric boundary must be the same on both sides of the boundary. This requirement is the same as the statement that k_r must be continuous across the boundary. Then the exponentially decaying near-field waves, with their short wave front spacing, will refract only into supercritical angles into medium 3.

For fluorophores close to the surface, exponentially decaying waves with a wide range of decay constants ik_z will extend to the surface, giving rise to a wide band of supercritical refraction angles. However, for fluorophores somewhat farther away, only those exponentially decaying waves with the longest decay distances (i.e., the smallest ik_z) will reach the surface, giving rise to a rather narrow band of supercritical emission angles extending only slightly above the critical angle. Therefore, by viewing only supercritical angle emission at a fixed angle θ, one will detect only fluorophores near the surface. The higher the θ, the closer to the surface are the detected fluorophores.

One *might* conclude that (1) at any particular supercritical observation angle θ in the glass, the observed intensity will decrease exponentially with z as a fluorophore is pulled away from the surface; and (2) the total emission into all other angular ranges is unaffected by moving the fluorophore. However, neither of these conclusions is correct. Recall that a fluorophore must be modeled as a fixed-power, rather than fixed-amplitude, dipole. This means that any increase in emitted power into any one set of directions, for example, supercritical angles into the glass, will be at the expense of emitted power into other directions. Furthermore, the intensity emitted into medium 1 is determined partly by the phase-dependent interference between direct and reflected plane waves, which is also a function of z. The intensity at any angle must be normalized by a function describing the total power $P_T(z)$ released by the dipole (including any lost into heat in a dissipative medium 2). In general, $P_T(z)$ can be calculated from

$$P_T(z) = (\omega/2)\,\mathrm{Im}(\boldsymbol{\mu}\cdot\mathbf{E}') \tag{7.33}$$

Physically, this formula describes the power dissipated by a harmonic oscillator (the emission dipole with moment $\boldsymbol{\mu}$) as it is driven by the force felt at its own location from its own emitted and reflected electric field. P_T is calculable given all the refractive indices and Fresnel coefficients of the layered model.[12, 33]

Incorrect conclusion 1 above is sometimes said to derive from the "reciprocity principle," which states that light waves in any optical system all could be reversed in direction without altering any paths or intensities and remain consistent with physical reality (because Maxwell's equations are invariant under time reversal). Applying this principle here, one notes that an evanescent wave set up by a supercritical ray undergoing total internal reflection can excite a dipole with a power that decays exponentially with z. Then (by the reciprocity principle) an excited dipole should lead to a supercritical emitted beam intensity that also decays exponentially with z. Although this prediction would be true *if* the fluorophore were a fixed-amplitude dipole in both cases, it cannot be modeled as such in the latter case.

The radiated intensity $\hat{S}(\mathbf{r}, z)$ from a fluorophore near a surface per unit

of adsorbed power can be derived from the Poynting vector magnitude. In terms of $\mathbf{E}_1'(\mathbf{r})$ and $\mathbf{E}_3'(\mathbf{r})$, it is

$$\hat{S}_i(\mathbf{r}, z) = \frac{cn_i\,|\mathbf{E}_i'(\mathbf{r}, z)|^2}{8\pi P_T(z)} \tag{7.34}$$

where c is the speed of light in vacuum. If we multiply $\hat{S}$ by the input power to the fluorophore's absorption dipole, then (assuming a 100% quantum yield) we get the intensity $I'(\mathbf{r}, z)$ radiated from the fluorophore:

$$I_i'(\mathbf{r}, z) = |\boldsymbol{\mu}_a\cdot\mathbf{E}|^2\,\hat{S}_i(\mathbf{r}, z) \tag{7.35}$$

Two additional feature can be incorporated into Eqs. (7.32)–(7.35): the dipole orientation distribution and the concentration distribution in systems consisting of many dipoles. The orientation of the dipole with respect to the surface, described by angles $\Omega' \equiv (\theta', \phi')$, affects $\mathbf{E}_i'$ and all the other measurables derived from it.[33] Consider a concentration distribution of dipoles in both orientation and distance from the surface specified by $C(\theta', \phi', z)$. Since the dipoles all oscillate incoherently with respect to one another, the integrated intensity $\mathscr{I}$ due to this distribution is simply:

$$\mathscr{I}_i(\mathbf{r}) = K\int d\Omega'\,dz\,C(\Omega', z)\,I_i'(\mathbf{r}, \Omega', z) \tag{7.36}$$

The total fluorescence power $\mathscr{F}$ collected from the fluorophore distribution by a microscope objective centered in the normal line at a distance r is an integral of $\mathscr{I}$ over the objective's aperture which subtends a solid angle Ω:

$$\mathscr{F}_i(r) = \int r^2\,d\Omega\,\mathscr{I}_i(\mathbf{r}) \tag{7.37}$$

Returning to the case of a single dipole, we find another parameter to be useful: the fluorescence collection efficiency Q. Parameter Q is the fraction of the total energy dissipated by a fixed-power dipole that is collected by a microscope objective centered on the normal at distance r:

$$Q(z, \theta') \equiv \frac{\text{collected power}}{\text{total dissipated power}} = \int r^2\,d\Omega\,\hat{S}_i(\mathbf{r}, z, \theta') \tag{7.38}$$

Combining the above equations, we can write a useful expression for the collected fluorescence from a distribution of dipoles in terms of the collection efficiency Q for a single dipole:

$$\mathscr{F} = K\int dz\,d\Omega'\,C(z, \phi', \theta')\,|\boldsymbol{\mu}_a\cdot\mathbf{E}|^2\,Q(z, \theta') \tag{7.39}$$

As shown by Hellen and Axelrod,[33] $Q(z, \theta')$ can be written in terms of the Q fractions for dipoles which are perpendicular ($\perp, \theta' = 0$) and parallel ($\parallel, \theta' = \pi/2$) to the surface:

$$Q(z, \theta') = \left(\frac{Q^{\perp}(z)}{1 + \eta(z) \tan^2 \theta'} + \frac{Q^{\parallel}(z)}{1 + [\eta(z) \tan^2 \theta']^{-1}} \right) \tag{7.40}$$

where $\eta(z) \equiv P_T^{\parallel}/P_T^{\perp}$ is the ratio of the total power dissipated by fixed-amplitude dipoles oriented parallel ($\parallel$) to the interface to that dissipated by those oriented perpendicular ($\perp$) to the interface. Equation (7.40) shows that at each dipole distance the collected energy can be written as a weighted average of the collection efficiencies for perpendicular- and parallel-oriented dipoles.

7.3.3. Graphical Results

Rather than displaying the rather complicated explicit forms for P_T, η, Q, $\hat{S}$, $\mathscr{I}$, and $\mathscr{F}$ in general terms of η_i, t, Ω', Ω, and C, we show here graphical results for certain specific configurations based on numerical integration. The qualitative features of these results will be relevant for most other configurations. We specialize in two particular interfaces: bare glass/water, where the intermediate layer is just an extension of medium 3 (i.e., $n_2 = n_3$); and glass/aluminum film (22 nm thick)/water. We will assume that all the dipoles are oriented either parallel or perpendicular to the interface; this assumption will be extended to a random orientation distribution later.

Figure 7.3 shows the radiated intensity $\hat{S}$ as a function of the observation angle θ for a dipole 80 nm from the surface. For simplicity, the azimuthal angle of observation ϕ is averaged. (This is equivalent to assuming that the excited dipole distribution is azimuthally symmetric about the surface normal.)

In the bare glass case, note that a rather strong peak of intensity is drawn into the glass, maximal at exactly $\theta = \theta_c$, but with significant intensity into supercritical angles. The effect is especially pronounced for dipoles oriented perpendicular to the surface, but is present for any position or orientation distribution.

In the aluminum film case, a peak of intensity directed into the glass is again present, but here centered in an extremely narrow band at some $\theta = \theta_p > \theta_c$. Angle θ_p is called the "surface plasmon" angle and arises from near-field waves from the dipole whose radial k-vector magnitude k_r is exactly matched to resonant electronic vibrations which can propagate on the metal surface and then reemit light into the hollow cone pattern depicted.[13] Note that dipoles perpendicular to the metal surface can furnish energy into the surface plasmons quite effectively, leading to an apparent transmission of light through a virtually opaque metal film. However, dipoles parallel to the surface are very unsuccessful at coupling with surface plasmons, and almost all the radiated emission appears in the water.

To make any progress in calculating $\mathscr{F}$ from Eqs. (7.39) and (7.40), we must know the total powers $P_T^{\parallel,\perp}(z)$ and their ratio $\eta(z)$; these are shown in Figure 7.4. Note that for the bare glass case (Figure 7.4a), the power P_T

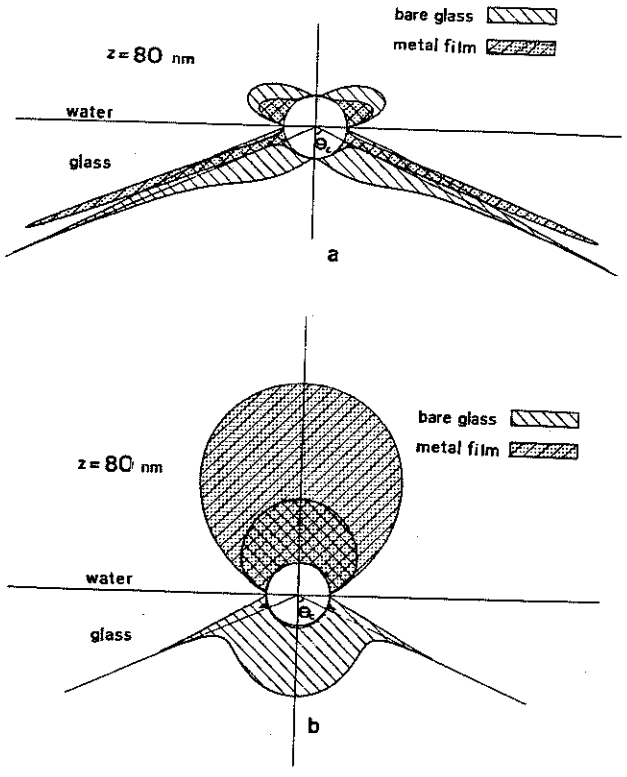

Figure 7.3. Intensity $\langle \hat{S} \rangle^{\parallel,\perp}$ versus polar observation angle θ for dipoles oriented perpendicular (a) and parallel (b) to the surface, normalized for constant total power of emission and averaged over the azimuthal angle of observation. The dipoles are assumed to be at $z = 80$ nm. At each angle, the radial distance from the center circle (surrounding the dipoles' location) is proportional to the radiated power. The bare glass case is a fused-silica ("glass")/water interface; the metal film case is a fused-silica/Al film (22 nm thick)/water interface. Parameters assumed are $\varepsilon_1 = 1.77$ ($n_1 = 1.33$); $\varepsilon_2 = -32.5 + 8.4i$; $\varepsilon_3 = 2.13$ ($n_3 = 1.46$); $\lambda_0 = 520$ nm. Note that at $z = 80$ nm from a metal film, the dipole is well out of range of surface quenching, and constructive interference with the reflected light actually increases the parallel dipole emission intensity into the water.

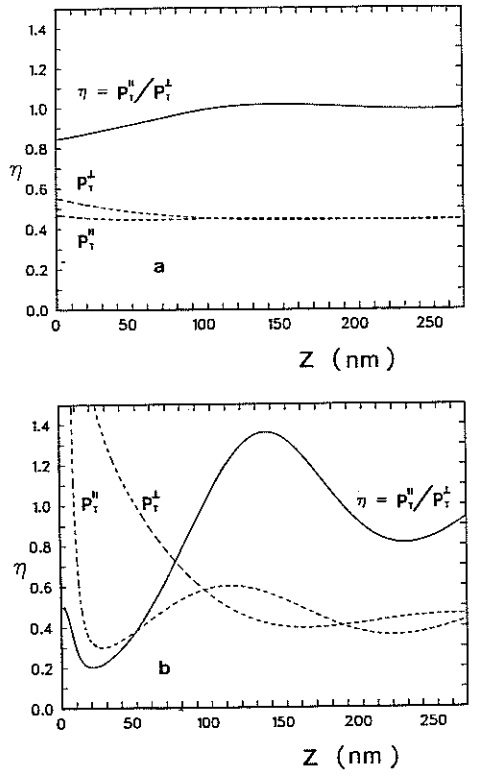

Figure 7.4. Total power P_T (in arbitrary units) dissipated by fixed-amplitude dipoles oriented parallel and perpendicular to the interface (——), and the ratio of these powers η (——) versus distance of the dipole z from the interface with medium 1, assumed to be water. (a) Bare glass; (b) aluminum film on glass. All optical parameters are the same as in Figure 7.3.

increases slightly for perpendicular dipoles very close to the surface. This corresponds to an approximately 10% decrease in the fluorescence lifetime of fluorophores. This effect should be taken into account when measuring fluorescence lifetimes near dielectric surfaces. For parallel dipoles, P_T exhibits only slight undulations.

Figure 7.4b shows P_T for the aluminum film case. There is a dramatic increase in P_T for both dipole orientations at small distances. Virtually all of that energy is converted into heat in the metal, thereby accounting for the strong fluorescence quenching on metal surfaces. For dipoles oriented parallel, an additional factor further promotes quenching: when the dipole is very near the surface ($z \ll \lambda$), its oppositely charged mirror image in the metal virtually cancels out the emitted electric field by simple wave interference.

The remaining variable required for calculation of $\mathcal{F}$ from Eqs. (7.39) and (7.40) is the collection efficiency Q, which measures the fraction of the total power emitted by a fluorophore that can be gathered as light by the microscope objective. Figure 7.5 shows $Q^{\parallel,\perp}$ for both parallel and perpendicular dipole orientations, for an objective positioned to look either through the water or through the glass substrate.

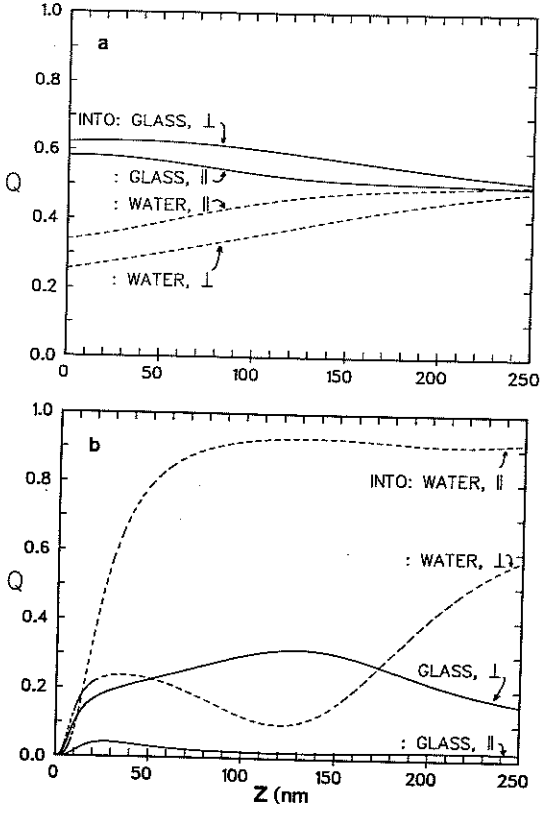

Figure 7.5. Collection efficiencies $Q^{\parallel,\perp}$ versus z, for an objective of numerical aperture 1.4 centered on the normal to the interface. Results are given both for the objective positioned "beneath" the interface to collect light emitted through the glass and "above" the interface to collect light emitted in the water. (a) Bare glass; (b) aluminum film on glass. All optical parameters are the same as in Figure 7.3.

Figure 7.5a shows the bare glass case. It shows that viewing through the glass substrate is more efficient than viewing through the water, at least for fluorophores very near the substrate surface. Around 60% of the emitted energy can be captured by a numerical aperture 1.4 objective by viewing through the glass substrate; only around 30% can be captured by viewing through the water. Much of this advantage is due to the ability of the high aperture to gather the emitted peak centered at $\theta = \theta_c$ (see Figure 7.3). For smaller aperture objectives, the relative advantage of viewing through the

substrate diminishes. Clearly, a 1.4-aperture objective is much better than a 1.3-aperture objective because of its special ability to gather the $\theta = \theta_c$ peak.

Figure 7.5b shows the aluminum film case. In the example shown, the surface plasmon peak is gathered (but just barely) by the objective; if it were not, the collected emission into the glass would be much less. However, even with this high aperture, it is still more efficient to view the fluorophores through the water for most distances outside the strong quenching region of $z < 10$ nm. For large z distances, viewing through the water is very efficient. This is simply because the metal surface acts like a mirror for far-field propagating light emitted by the dipole.

Figure 7.6 shows the intensity I that would be detected in the glass at a particular supercritical angle, given an excitation intensity that is *not* a function of z (e.g., epi-illumination rather than TIR). Only the results for perpendicular dipoles are shown (so that averaging over azimuthal ϕ is unnecessary). The result for parallel dipoles is qualitatively similar except that the metal film case would be very much reduced in overall intensity.

In the bare glass case, note that the decay is not exponential, as otherwise would be expected if the "reciprocity principle" had been misapplied here. Nevertheless, by viewing only supercritical angles, one can selectively observe only those fluorophores within several hundred nanometers of the surface, even if the excitation (rather than the emission) is not surface-selective at all.

In the metal film case, the intensity is virtually zero for distances less than 5 nm. This quenching effect occurs at all angles, not just supercritical ones. The excitation energy is almost entirely converted into heat in the metal film. At larger distances, the dipole near field couples with surface plasmons whose emission into the glass is centered around $\theta = \theta_p$. At even larger distances, the near field is too weak to interact with the surface, and the supercritical intensity drops toward zero.

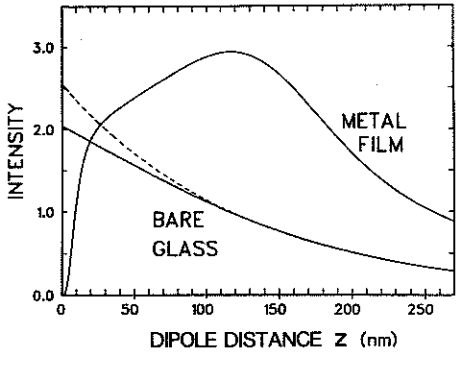

Figure 7.6. Intensity emitted at supercritical angle $\theta = 70°$ into the glass versus dipole distance z for dipoles oriented perpendicular to the interface. The solid lines show the properly normalized (fixed-power dipole) intensities for the bare glass and Al film surfaces. The dashed line shows the exponentially decaying intensity that would be obtained for bare glass by omitting the required normalization P_T in Eq. (7.34). All optical parameters are the same as in Figure 7.3.

7.3.4. Theoretical Results for a Distribution of Dipoles: Random Orientations

The collected fluorescence $\mathcal{F}$ [from Eq. (7.39)] clearly depends on the orientation distribution of the dipoles and the incident polarization through the dependences on θ' and $\mathbf{E}$. We will assume a special but common case here: randomly oriented dipoles with a z-dependent concentration near the surface, excited by a p-polarized evanescent wave.

In this case, $C(z, \phi', \theta') = C(z)$. Equation (7.39) can then be written as an integral over the dipole distance z:

$$\mathcal{F} = K(\mu_a)^2 \int dz\, C(z)\, |E_p(z)|^2 \left[w^{\perp}(z)\, Q^{\perp}(z) + w^{\parallel}(z)\, Q^{\parallel}(z)\right] \qquad (7.41)$$

where the weighting terms $w^{\parallel,\perp}$ depend in general upon the excitation polarization. For the case here, in which the incident polarization is p and the absorption dipole $\boldsymbol{\mu}_a$ is parallel to the emission dipole $\boldsymbol{\mu}$, these weightings are

$$w^{\parallel,\perp}(z) = |\alpha_x|^2\, w_x^{\parallel,\perp}(z) + |\alpha_z|^2\, w_z^{\parallel,\perp}(z) \qquad (7.42)$$

where the $\alpha_{x,z}$ factors determine the amplitude of the $\hat{x}$- and $\hat{z}$-components of the excitation field as given in Eq. (7.12). (The form of $\alpha_{x,z}$ shown in Eq. (7.12) corrects a misprint in Eq. 56 of Ref. 33.) The $w_{x,y,z}^{\parallel,\perp}(z)$ weighting factors, written out explicitly by Hellen and Axelrod[33] for the randomly oriented dipole case, are functions of $\eta(z)$ and are depicted in Figure 7.7.

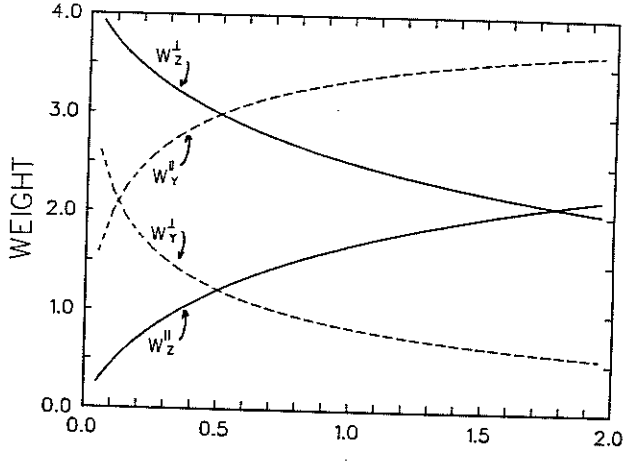

Figure 7.7. The weightings $w_{y,z}^{\parallel,\perp}$ versus $\eta(z)$ for the special case of p-polarized incident light and randomly oriented dipoles. In this case, $w_x^{\parallel,\perp} = w_y^{\parallel,\perp}$.

The remaining functions of z that are needed in order to do the integral in Eq. (7.41) are the excitation intensity $|E_p(z)|^2$ and the concentration profile $C(z)$. The excitation intensity is easily obtained from Eq. (7.10). Note that the $\exp(-z/d)$ implicit in the $|E(z)|^2$ factor can be written as $\exp(-zk_1\beta)$, where

$$k_1 \equiv 2\pi n_1/\lambda_0$$
$$\beta \equiv (2/n)(\sin^2\theta - n^2)^{1/2} \tag{7.43}$$

so that $(\beta k_1)^{-1} = d$, the evanescent wave depth.

The concentration profile may be known, for example, a delta function at a particular z (say, $z=0$) for closely adsorbed material, or a step function out to a particular $z>0$. However, often, to deduce $C(z)$ may be the purpose of the whole exercise. Equation (7.41) can be cast into a form which is similar, but not equivalent to, a Laplace transform of the concentration profile $C(z)$. Variables $w^{\parallel,\perp}$ and $E_p(0)$ in the integrand of Eq. (7.41) are functions of β, since they are all functions of the incidence angle θ. Then Eq. (7.41) can be written as

$$\mathscr{F} = \int_0^\infty dz \exp(-\beta k_1 z)\, C(z)\, h(z, \beta) \tag{7.44}$$

where

$$h(z, \beta) \equiv K(\mu_a)^2\, |E_p(0, \beta)|^2\, [w^\perp(z, \beta)\, Q^\perp(z) + w^\parallel(z, \beta)\, Q^\parallel(z)] \tag{7.45}$$

The presence of the $h(z, \beta)$ factor makes Eq. (7.44) different from a Laplace transform of $C(z)$. If the z dependence of $h(z, \beta)$ is ignored,[34–36] then calculated concentrations of fluorophore near an interface derived from collected fluorescence are approximations. Also, the β dependence in the $w^{\perp,\parallel}$ causes the integral in Eq. (7.44) to differ from the form of a Laplace transform even after the excitation term is factored out.

If the excitation electric field is an s-polarized evanescent field instead of the above p-polarized example, then $w^{\perp,\parallel}$ [$= w_y^{\perp,\parallel}(z)$] does not depend upon β. Therefore, an approximate $C(z)$ can be calculated from the observed fluorescence $\mathscr{F}(\beta)$ (obtained experimentally by varying θ) by ignoring the z dependence in the bracketed term in Eq. (7.45) and by inverse Laplace transforming Eq. (7.44) after the $|E_s(0, \beta)|^2$ term has been factored out.[37–39]

7.3.5. Consequences for Experiments

7.3.5.1. Polarization

A complete treatment[33] shows the polarizations of the emitted fields from single dipoles, but the polarization from an orientational and spatial distribution of dipoles, presumably calculated by numerical integration in particular cases, has yet to be done. The graphs in Sections 7.3.3 and 7.3.4 above assume that no polarizing analyzer is used. The polarization field of each emitting dipole in a distribution is always in the same plane as that dipole's orientation at the instant of emission and perpendicular to the direction of emitted light propagation. However, the polarization from excited dipoles spread over an orientational distribution near an interface in general will be different from that observed from an identical distribution far from an interface, because the emission collection efficiency from a dipole at an interface depends upon dipole orientation and distance from the surface (see Figure 7.5). An additional complication is that the polarization will depend upon the angle of observation and therefore will be a function of the numerical aperture of the collecting lens.

7.3.5.2. Fluorescence Efficiency and Lifetime

The preceding treatment assumed, for simplicity, that the quantum yield of the isolated dipole (i.e., at $z=\infty$) was 100%. Here we assign it a more general value of q_0. The following definitions are useful:

$$p \equiv P_T(z)/P_T(\infty)$$
$$f \equiv \frac{\int d\Omega\, S(z, \Omega)}{\int d\Omega\, S(\infty, \Omega)} \tag{7.46}$$

Both p and f are ratios of a power emitted at position z relative to that for an isolated dipole; p refers to total power (light plus heat) whereas f refers to radiated power only, derived by integrating the fixed-amplitude dipole radiated intensity S [given by Eq. (7.34) without the P_T normalization in the denominator] over 4π steradians.

We seek an expression for the actual quantum efficiency observed for a fluorophore at distance z, which we denote as q. One can show that

$$\frac{1}{q} = \frac{1}{f} \cdot \left(\frac{1}{q_0} + p - 1\right) \tag{7.47}$$

Given a "natural" (i.e., no radiationless decay) fluorescence lifetime τ_0 for an isolated fluorophore, one can show that the actual observed lifetime for a real fluorophore near an interface is

$$\tau = q\tau_0/f \tag{7.48}$$

Note that this expression differs from the more familiar $\tau = q\tau_0$ applicable to systems in which the rate constant of the fluorescence emission path to the

ground state is constant and alterations in the fluorescence power arise only from changes in the radiationless decay rate. Near a surface, however, the fluorescence is affected in three ways: (1) the radiated power rate can change due to interference between the dipole's reflected and directly emitted fields; (2) the near field of the dipole, which normally carries away no energy, may be converted into a radiating field in the denser medium by interaction with the surface; and (3) the surface may be a dissipative medium, such as a real metal, thereby converting the dipole near field into heat. In most cases with $z < 10$ nm, effects 2 and 3 combine to increase the total dissipated power P_T, hence decreasing the lifetime for fluorophores close to the surface. Note that the degree of lifetime shortening does depend on the orientation of the dipole.

It is possible in principle for effect 1 to exert an opposing effect by tending to decrease P_T through destructive interference between the reflected and direct fields. However, for most materials likely to be encountered, either dielectrics or metals, the net result will be a lifetime decrease, not an increase, for small z.

For bare glass, the lifetime decrease is only slight ($\sim 10\%$ for $q_0 = 1$ and 5% for $q_0 = 0.5$); for metal-coated glass, the effect is dramatic. Particularly on metals, the expected decrease in lifetime may help protect the fluorophore against photobleaching that arises from excited-state chemical reactions involving diffusional collisions.

7.3.5.3. Collection System Design

The significant anisotropy in the emission pattern from a fluorophore near a surface (Figure 7.3) suggests how to maximize the collection of emitted light. When viewing through the glass, it is clearly desirable to use an objective with a numerical aperture (N.A.) high enough to collect the sharp peaks in the pattern.

For a bare glass/water interface, this criterion is

$$\text{N.A.} > n_1 = 1.33 \tag{7.49}$$

For a glass/metal film/water interface, this criterion is

$$\text{N.A.} > \text{Re}\left[\left(\frac{\varepsilon_1 \varepsilon_2}{\varepsilon_1 + \varepsilon_2}\right)^{1/2}\right] \tag{7.50}$$

This condition predicts that N.A. = 1.4 would capture the surface plasmon peak from an aluminum film surface but not from a silver-film surface. Therefore, since objectives with aperture higher than 1.4 are rather rare, an aluminum film is a better choice.

7.3.5.4. Selective Detection of Adsorbed Fluorophores

On bare glass, the supercritical angle emission that occurs only from fluorophores near the glass suggests a method of selective detection of such fluorophores even in the presence of excited fluorophores farther out in the solution. A microscope objective with a high numerical aperture (e.g., 1.4) can be masked at its back focal plane to exclude any emission at less than the critical angle into the glass, thereby excluding all light from distant fluorophores. This approach avoids the necessity of selective excitation near the surface, as is done by evanescent wave excitation. However, an appropriately masked objective (at an accessible plane in the microscope equivalent to the back focal plane) appears in practice to provide rather poor resolution.

7.3.5.5. Selective Surface Quenching

On a metal-coated surface, the highly effective and highly z-dependent quenching could be used to distinguish between fluorophores close to the surface (e.g., $z < 2$ nm, strongly quenched) and those farther out (e.g., $z > 7$ nm, only weakly quenched). For example, a metal-coated surface could be coated with an artificial, reconstituted, or flattened biological phospholipid bilayer membrane. Fluorescence from the more distal bilayer half would not be quenched nearly so strongly as that from the proximal half. This possibility of selectively detecting fluorophores in only one half of a bilayer may find application to studies of membrane asymmetry, transmembrane transport, and lipid "flip-flop." This selective quenching can be used quite generally, since an aluminum-coated surface can be chemically treated with organosilanes to derivatize it with a wide range of functionalities (see Section 7.4.5).

Metal coatings are subject to heating more than dielectric coatings because, for most incidence angles, a significant portion of the incident light can be absorbed. At high but accessible incident focused laser intensities, microscopic boiling in the water can be seen. As a general rule, the incident laser intensity should be reduced by at least two orders of magnitude from this point.

Semiconductor surfaces also quench nearby fluorescence. This effect has been applied experimentally[40] but not yet treated theoretically.

7.4. TIRF for a Microscope

A wide range of optical arrangements for TIRF have been employed, both with and without a microscope.[5] The arrangements coupled to a

microscope[41] are particularly appropriate where small observation and illumination areas are required, for example, for examining biological cells and for measuring local adsorption kinetic and surface diffusion rates.

7.4.1. Inverted Microscope

Figure 7.8 shows a possible arrangement for an inverted microscope. This arrangement is fairly easily switched to phase contrast transmitted illumination or to conventional epi-fluorescence and is also usable with even the shortest working distance objectives. The key element in the optical system is an optical glass or fused-silica cubical prism that permits the incident laser beam to strike the TIR interface (which may be the surface of a microscope slide or coverslip placed in optical contact with the prism via a drop of immersion oil or glycerol) at greater than the critical angle. This prism need not be matched in refractive index to the TIR interface material nor need it be cubical. As an illustration of the optical effect seen with this setup, Figure 7.9 shows a fibroblast in culture labeled with a lipid probe. TIRF clearly illuminates with high contrast only the surface-contacting regions of the cell.

Other TIRF configurations for inverted microscopes have been employed. Figure 7.10 shows an alternative system.[42] Instead of a prism fixed with respect to the beam as above, the prism is fixed with respect to the sample. The glass slide substrate propagates the incident beam toward the

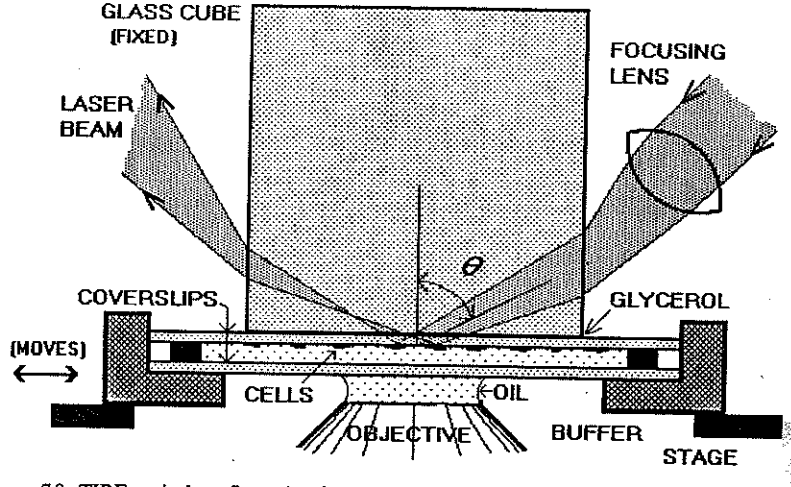

Figure 7.8. TIRF optical configuration for an inverted microscope; detail of the sample chamber region.

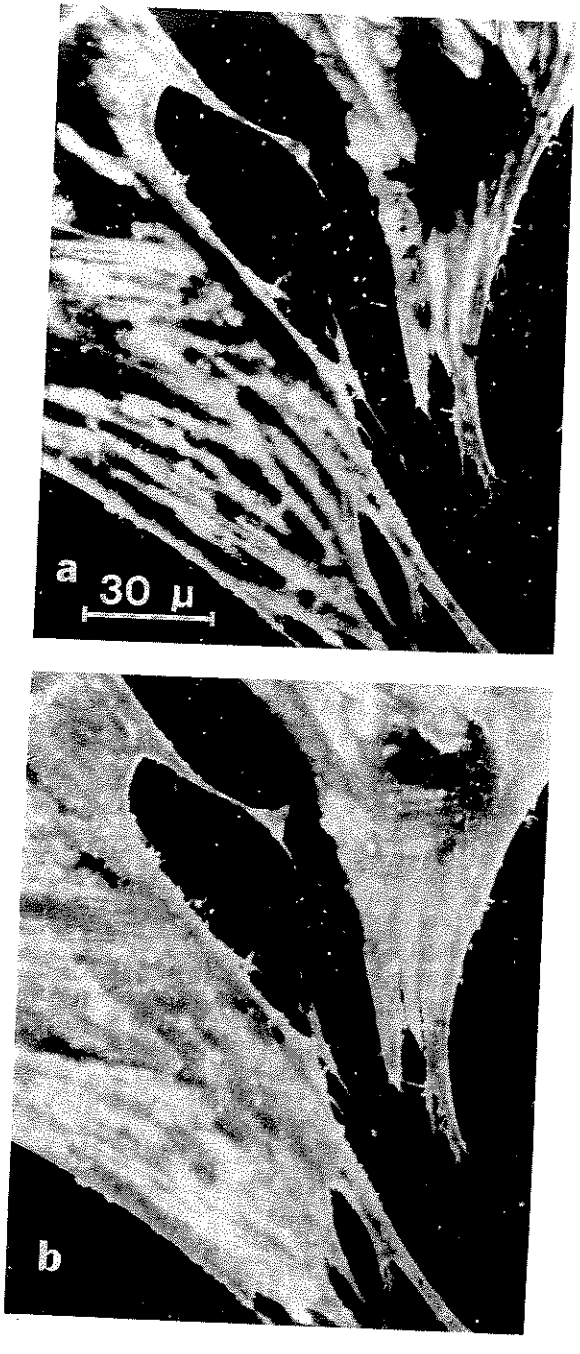

Figure 7.9. Human skin fibroblasts labeled with diI and illuminated by TIRF at two different angles of incidence. (a) $\theta = 74.3°$, $d = 105$ nm; (b) $\theta = 67.9°$, $d = 406$ nm. In this setup, $\theta_c = 67.5°$. Notice how more of the cell surface is immersed in the deeper evanescent wave of (b).

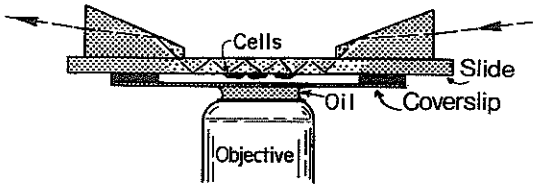

Figure 7.10. TIRF microscopy with prisms fixed to the substrate plate. (Adapted from Weis *et al.*[42])

microscope's optical axis via multiple internal reflections. The illuminated TIRF area will move with translation of the sample in this system.

7.4.2. Upright Microscope

Figure 7.11 shows a TIRF arrangement for an upright microscope. This setup is particularly appropriate for viewing culture cells growing in standard plastic culture dishes. The prism is a trapezoid (actually, a truncated 60° equilateral triangle made of high-refractive index flint glass) brought into optical contact (via a drop of oil or glycerol) with the bottom of the culture dish. This arrangement has the advantage that (1) the culture dish can be inserted and removed easily; and (2) the illuminated region does not move when the microscope is focused. It has the disadvantage that the incidence angle is not variable.

7.4.3. Prismless TIRF

By using an objective with a high numerical aperture (generally, 1.4), supercritical angle incident light can be cast upon the sample by epi-elluminationthrough the objective.[43] The incident beam must be constrained to pass through the periphery of the objective's pupil and must emerge with only a narrow spread of angles; this can be accomplished by ensuring that the incident beam is focused off-axis at the objective's back focal plane. It emerges into the immersion oil ($n_3 = 1.52$) at a maximum angle θ given by

$$\text{N.A.} = n_3 \sin\theta \tag{7.51}$$

For total internal reflection to take place at the sample surface, θ must be greater than the critical angle θ_c, given by

$$n_1 = n_{\text{water}} = 1.33 = n_3 \sin\theta_c \tag{7.52}$$

From Eqs. (7.51) and (7.52), it is evident that N.A. must be greater than 1.33, preferably by a substantial margin. Several possible arrangements are shown

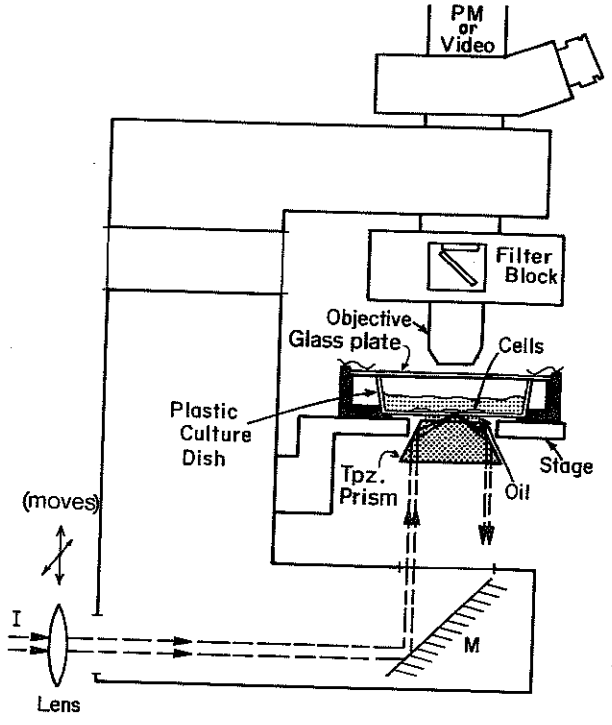

Figure 7.11. TIRF adapted to an upright microscope, shown here with a special sample chamber for long-term viewing of cells in a plastic tissue culture dish. The prism is a truncated equilateral triangle. The region of the sample chamber is shown enlarged relative to the rest of the microscope for pictorial clarity. The sample chamber is provided with a slow flow of humidified 5% CO_2/air, and 37°C air is blown over the whole region.

in Figure 7.12, one of which even can utilize a conventional arc source rather than a laser beam.

7.4.4. TIRF Interference Fringes

By intersecting two laser beams at the TIR surface, finely spaced interference fringes can be produced. These fringes are useful for studies of surface diffusion rates, as discussed in Section 7.5.6. The interfringe (peak-to-peak) spacing is $\lambda_0[2n_3 \sin\theta \sin(\beta/2)]^{-1}$, where β is the intersection angle between the two beams in the plane of the TIR surface. TIRF fringes were first introduced by Weis *et al.*[42] as an aid to focusing on the TIRF surface.

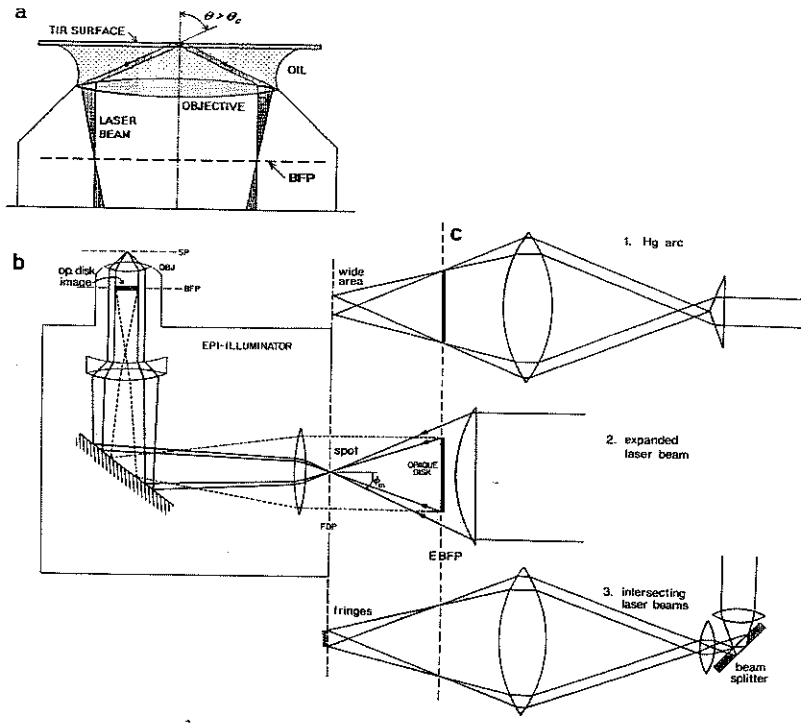

Figure 7.12. Optical arrangements for three prismless TIRF configurations through a 1.4-aperture microscope objective. Abbreviations: SP, Sample plane; OBJ, objective lens; BFP, back focal plane of the objective; EBFP, equivalent back focal plane outside the microscope; FDP, field diaphragm plane. Any sharp feature at the EBFP will form a sharp image at the BFP; likewise for the FDP and the SP (the TIR surface). Panels a (detail of the objective) and b (detail of the epi-illuminator) are common for all three configurations; panel c shows each in the region upbeam from the epi-illuminator: (1) mercury arc source, including the use of a conical lens to increase the power of supercritical light at the expense of subcritical light; (2) laser source focused to a spot with a single focusing lens; (3) laser source split into two mutually coherent beams which intersect at the FDP, forming two evanescent beams intersecting at 180° at the sample plane. This produces a TIR fringe pattern with a submicroscopic 0.18-μm internode spacing. Additional configurations are given in Ref. 43.

Figure 7.12c shows intersecting beam TIRF based around a prismless system, as discussed above, with a high-aperture object. This system is mechanically very stable, enabling one to achieve interfringe spacings of $\sim$0.18 μm without the blurring effects of small vibrations. Another arrangement uses a parabolic mirror to direct the intersecting beams into a hemispherical prism (see Figure 7.15); although somewhat more awkward, this system allows a wider range of incidence angles.

7.4.5. General Experimental Suggestions

Regardless of the optical configuration chosen, the following suggestions may be helpful:

1. The prism used to couple the light into the system and the (usually disposable) slide or coverslip in which TIR takes place need not be matched exactly in refractive index.
2. The prism and slide may be optically coupled with glycerol, cyclohexanol, or microscope immersion oil, among other liquids. Immersion oil has a higher refractive index (thereby avoiding possible TIR at the prism/coupling liquid interface at low incidence angles), but it tends to be more autofluorescent (even the "extremely low" fluorescence types).
3. The prism and slide can both be made of ordinary optical glass for many applications, unless shorter penetration depths arising from higher refractive indices are desired. Optical glass does not transmit light below about 310 nm and also has a dim autoluminescence with a long (several hundred microsecond) decay time, which can be a problem in some photobleaching experiments. The autoluminescence of high-quality fused silica (often called "quartz") is much lower. Tissue culture dish plastic (particularly convenient as a substrate in the upright microscope setup) is also suitable, but tends to have a significant autofluorescence compared to ordinary glass. More exotic high-n_3 materials such as sapphire, titanium dioxide, and strontium titanate can yield exponential decay depths d as low as $\lambda_0/20$.
4. The TIR surface need not be specially polished: the smoothness of a standard commercial microscope slide is adequate.
5. Illumination of surface-adsorbed proteins can lead to apparent photochemically induced cross-linking. This effect is observed as a slow, continual, illumination-dependent increase in the observed fluorescence. It can be inhibited by deoxygenation (aided by the use of an O_2-consuming enzyme/substrate system such as protocatechuic deoxygenase/protocatechuic acid or glucose/glucose oxidase) or by 0.05 M cysteamine. Photobleaching, which produces a slow decrease in fluorescence, can be reduced by deoxygenation as above or by 0.01 M sodium dithionite, among other substances.[44–49]
6. Virtually any laser with a total visible output in the 0.5 W or greater range should be adequate. The most popular laser for cell biological work with a microscope appears to be a 3-W continuous-wave argon laser.
7. TIRF experiments often involve specially coated substrates. A glass surface can be chemically derivatized to yield special physi- or

chemisorptive properties. Covalent attachment of certain specific chemicals is particularly useful in cell biology and biophysics; such chemicals include poly-L-lysine for enhanced adherence of cells; hydrocarbon chains for hydrophobicizing the surface in preparation for lipid monolayer adsorption; and antibodies, antigens, or lectins for producing specific reactivities.

Covalent derivatization generally involves pretreatment by an organosilane (see the catalog of Petrarch Systems). The protocol for covalent poly-L-lysine attachment to planar glass slides is similar to that described for the treatment of spherical glass beads.[50] The protocol for preparing lipid monolayers on hydrophobic glass is given by VonTscharner and McConnell.[51] Methods for preparing model membranes on planar surfaces suitable for TIR have been reviewed.[52–54]

Aluminum coating (for surface fluorescence quenching; see Section 7.3.5.5) can be accomplished in a standard vacuum evaporator; the amount of deposition can be made reproducible by completely evaporating a premeasured constant amount of aluminum. After deposition, the upper surface of the aluminum film spontaneously oxidizes in air very rapidly. This aluminum oxide layer appears to have some similar chemical properties to the silicon dioxide of a glass surface; it can be derivatized by organosilanes in much the same manner.

7.5. Applications of TIRF

7.5.1. Binding of Proteins and Probes to Artificial Surfaces

TIRF has been used to study equilibrium adsorption of proteins to artificial surfaces both to learn about the surface properties of various biomaterials that have medical applications and also to test the TIRF technique itself.

Several studies of the binding equilibria, kinetics, and conformational changes of proteins upon adsorption have employed extrinsic fluorophores attached to protein.[55–61] It is possible in principle that such extrinsic groups might themselves affect the adsorption process being investigated. To avoid this possibility, the intrinsic fluorescence of tryptophan or tyrosine residues in the protein can be monitored upon excitation by a $\lambda_0 = 280$ nm evanescent wave.[62–67] In certain cases, however, the greater susceptibility of proteins to photodegradation under UV illumination may outweigh the natural advantage of intrinsic fluorescence excitation.

Calibration of a TIRF intensity to derive an absolute concentration of adsorbate is a nontrivial problem, mainly because fluorescence quantum

efficiencies are apt to change upon adsorption to a surface. One route around this problem is to measure the depletion of bulk solute (in epi-illumination mode or in a standard spectrofluorimeter) when it is allowed to adsorb onto a known surface area.[58] Hlady *et al.*[68] proposed another method for the approximate calibration of TIR fluorescence. This method, involving use of nonadsorbing species as standards and ^{125}I-labeled protein with a γ-detection system, introduces a small correction for incident light scattered beyond the evanescent wave volume and for changes in the fluorescence emission quantum efficiency of proteins upon adsorption. A third method[57] is self-contained, in the sense that no other measuring instruments outside the TIRF system are needed. The total fluorescence is due to a bulk dissolved contribution plus a surface contribution. Since the bulk concentration is usually known, we need only measure its fractional contribution to the total fluorescence to calculate the surface concentration (approximating that quantum and collection efficiencies are unchanged upon adsorption). The fractional contribution can be deduced simply either by abolishing the fluorescence from the surface (with a strong photobleaching pulse of incident light) or by replacing the solution with a fluorescence-free rinse. In either case, the method works only if the time scale of the reversible adsorption kinetics is much longer than the time of the bleaching pulse or the change of solution.

TIRF for the sensing of protein adsorption can be transformed into a practical medical procedure.[69–76] Designed to serve as a continuous sensor element in a remote sample, a single multimode optical fiber or planar waveguide both supports the evanescent wave on its surface used for excitation and also guides the captured near-field fluorescence which propagates into the fiber at greater than the critical angle.[77] To make the fiber biochemically specific, it is covalently coated with either an antibody or its complementary protein antigen. When introduced into the target liquid, the antigen, or its complementary antibody, specifically adsorbs. In some of these cases, the intrinsic fluorescence of tryptophan is used to assay specific adsorption onto the optical fiber. Further experimentation will show whether the increase of fluorescence resulting from specific binding will be evident above a large background of nonspecifically adsorbed protein fluorescence likely to be encountered in biological fluids.

If the soluble protein that specifically adsorbs to the fiber can be extrinsically labeled, the background problem can be avoided. Of course, *in vivo* proteins cannot be labeled. However, it is conceivable that a protein labeled with a bulky extrinsic group (e.g., fluorescent dextrans) could be confined by a molecular sieve membrane (e.g., a dialysis membrane) within a closed volume surrounding the specifically derivatized optical fiber. When exposed to the (unlabeled) protein in the biological fluid under investigation, the membrane-clad fiber would allow some unlabeled protein to permeate in and

thereby compete with the confined fluorescent protein for surface binding sites.

Binding competition between a fluorescent and nonfluorescent species is the basis of a fluorosensor designed for detecting the presence of acetylcholine receptor (AChR) agonists and antagonists in solution.[78] Acetylcholine receptors are noncovalently but firmly attached to the optical fiber, and the target solution is spiked with a low concentration of the specific blocker α-bungarotoxin, labeled with fluorescein. It is found that the binding of the fluorescein bungarotoxin, as measured by TIRF through the fiber, is inhibited by the presence of known AChR agonists and antagonists.

By treating a glass surface with immobilized anti-human serum albumin (HSA) immunoglobulin in distinct spots, a spatially resolved TIRF pattern due to fluorescein-HSA binding from solution could be focused onto a CCD camera.[79] This spatially resolved TIRF technique offers the possibility of an internal control against background binding (giving rise to fluorescence between spots) and detecting the presence of several solution components simultaneously.

Some studies have used dye molecules themselves, rather than dye–protein conjugates, to investigate the surface charge properties of a solid/liquid interface. The emission spectra contain information on the hydrophobicity of the fluorophore environment. By studying the detailed structure of the vibronic bands of adsorbed pyrene at both a solid/liquid interface (using TIRF) and the corresponding solid/vapor interface, Hartner *et al.*[80] concluded that TIRF did successfully report the microenvironment of the adsorbed (rather than bulk) pyrene. The adsorption of a dye molecule at an SnO_2 thin film as a function of pH was measured.[81] Investigation of TIR-excited emission shifts of an adsorbed dye has successfully detected hydrophobicity gradients on silica surfaces which appear correlated with the ability of each local region to adsorb blood albumin protein.[82]

By preparing planar lipid monolayers or bilayers on hydrophobically derivatized or native hydrophilic glass, respectively, the adsorption equilibrium constants of a blood coagulation cascade protein, prothrombin, have been examined by TIRF on a surface that more closely models actual cell surfaces and is amenable to alterations of surface charge. It was found that membranes of phosphatidylcholine (PC) that contain some phosphatidylserine (PS) bind prothrombin more strongly than pure PC membranes.[83]

Most of the early TIRF work with proteins at surfaces involved nonspecific adsorption. Recently, Poglitsch and Thompson[84, 85] have shown that TIRF can also detect specific but still reversible ligand–receptor binding at a planar lipid membrane on a solid glass support. Macrophage Fc receptors were successfully reconstituted into supported lipid monolayers, and the equilibrium binding constant of fluorescent-labeled monoclonal Fab fragments of immunoglobulin G (IgG) was measured by TIRF. By using the competition

with a labeled species (rhodamine-Fab) to measure binding strength of an unlabeled species (Fc-containing IgG), these authors were able to report an association constant between unlabeled polyclonal IgG and the reconstituted Fc receptors. Equilibrium binding constants of the antigen-binding site of both divalent monoclonal antibody and its Fab fragment on supported planar lipid monolayers doped with hapten-derivatized lipid were also obtained with TIRF, and the divalent antibody results were compared with theoretical models of two-step binding.[86]

7.5.2. Concentration of Molecules near Surfaces

The concentration of a solute or adsorbate may be a nontrivial function of the distance to the surface, a function which contains information about the thermodynamics of the surface interaction. To explore the fluorophore concentration $C(z)$ as a function of distance z from the surface, one can record the observed fluorescent intensity F as the characteristic depth d of the evanescent wave is varied. The mathematics of this is discussed immediately following Eqs. (7.44) and (7.45) above.

To vary d [or the related parameter β in Eqs. (7.44) and (7.45)], the angle of incidence θ can be varied. Experimentally, this is not trivial, because d is a very strong function of θ within only a few degrees greater than θ_c, and therefore θ must be measured to fractions of a degree. In addition, the presence of a solute (or the cytoplasm of a biological cell) alters the refractive index n_1 from its pure water value, and this altered value must also be known accurately. Rondelez *et al.*[87] have measured $F(d)$ versus θ to obtain information on the z-dependent concentration profile of artificial polymers adsorbed to glass or silica. Reichert *et al.*[88] have tested this approach, first with a fluorescein solution which was presumed to have a constant C independent of z, and second with a layer of fluorescein-labeled immunoglobulin adsorbed to quartz which was presumed to have a step-function $C(z)$. The theoretical expectations here are an approximation since their theory omits the normalization step discussed in Section 7.3. This omission, although not exactly correct, simplifies the calculation of $C(z)$ by converting it to an inverse Laplace transform of the observed fluorescence. The ability of this general approach to correctly report concentration profiles was checked on planes of fluorophores deposited in steps between layers of Langmuir–Blodgett films.[89]

A similar simplifying assumption has been used by Allain *et al.*[90] in analyzing their experiments on a flexible fluorescent anthracene–polystyrene copolymer coil in the vicinity of a nonadsorbing wall. The analysis appears to confirm a local decrease in $C(z)$ for small z at the solid/solution interface. Such a depletion layer is interpreted in terms of an "entropic repulsion"

model, whereby certain conformations of polymer are sterically prohibited near the surface.

Another method of obtaining $C(z)$ involves varying the angle at which the emission is observed. As discussed in Section 7.3, the near field of the emitting dipole can produce propagating light at supercritical angles in the glass; the smaller the dipole distance z to the surface is, the greater the intensity and the wider the range of angles that are cast into the supercritical zone. Each supercritical observation angle represents a different (but, for a nonmetallic surface, always monotonically decaying) dependence of collection efficiency versus z. The method of varying observation angle has been used by assuming that the monotonic decay is exponential (an approximation) to measure the concentration of a stiff, high-molecular-weight polysaccharide near a solid surface.[91] This application, using TIRF (but not requiring it) in a nonmicroscopic configuration, also indicated the presence of a surface depletion zone.

An unusual application of TIRF for measuring dye concentrations on a woven fabric of silk versus distance into the surface of the silk was reported by Kurahashi *et al.*[92] By comparing the relative intensities of silk's own fluorescence emission peak around 340 nm with that of the dye at longer wavelengths under both normal and TIR illumination, they concluded that the dye tends to concentrate in the interior bulk of the silk rather than on the surface. Although qualitatively clear, the spectra would have to be interpreted for the wavelength-dependent intensity of the evanescent wave and the significant light scattering to yield a more quantitative result.

7.5.3. Orientation, Rotation, and Fluorescence Lifetime of Molecules near Surfaces

The polarization properties of the evanescent wave[93] can be used to excite selected orientations of fluorophores, for example, fluorescent-labeled phosphatidylethanolamine embedded in lecithin monolayers on hydrophobic glass.[21] When interpreted according to an approximate theory, the total fluorescence gathered by a high-aperture objective for different evanescent polarizations gives a measure of the probe's orientational order. The polarization properties of the emission field itself, expressed in a properly normalized theory,[94] can also be used to determine features of the orientational distribution of fluorophores near a surface.

Both the physics and the chemistry of proximity to a surface can alter the excited-state lifetime and rotational motion of a fluorescent molecule. An extrinsic label attached to BSA has been found to reduce its fluorescence lifetime upon BSA adsorption to fused silica.[95] The decrease is too large to arise from the physical near-field proximity effects discussed in Section 7.3;

some sort of chemical conformational change or quenching due to high local concentrations upon adsorption might explain the effect. TIRF has been combined with time-resolved polarized anisotropy decay to measure molecular rotation rates in fluorescence-doped polystyrene double-layered films, mainly as a test of the selectivity of the results for the layer nearest the TIR sapphire prism.[96] Similar experiments on pyrene-containing poly(methyl methacrylate) films[97] showed that rotational rates of the probe were restricted near the surface relative to the bulk. In both cases, the "bulk" was not a low-viscosity liquid but a rigid polymer matrix. By a similar nonmicroscopic time-resolved TIRF technique, the rotational mobility of pyrene-labeled serum albumin adsorbed to artificial polymer films has been measured.[98]

Itaya *et al.*[99] have described a TIR system for obtaining time-resolved fluorescence decay curves induced by laser flash illumination of polymer films in a microscope configuration. Presumably, use of this configuration can be extended to studies on biological cells.

In these time-resolved studies, a simplified, non-normalized theory [i.e., effectively lacking the division by P_T in Eq. (7.34)] was used for comparison with the experimental results, so that the observed fluorescence from any region was assumed to be proportional to the local evanescent intensity in that region. A more precise analysis must take into account that distance from the interface affects the angular distribution of emission and that fluorescence lifetimes are necessarily affected by the proximity of the dielectric interface.

Many substances preferentially concentrate at interfaces, including liquid/liquid ones. Although TIRF is most easily adaptable to solid/liquid interfaces, Morrison and Weber[100] succeeded in observing the preferential adsorption of certain amphiphilic dyes at the interface between two immiscible and optically dissimilar liquids. Steady-state TIR fluorescence polarization in that system showed that the rotational diffusion of the interfacially adsorbed dye was restricted.

Fraaije *et al.*[101] have investigated the orientation of reversibly adsorbed cytochrome *c* as a function of experimentally controlled electrical surface potential. This project contains a number of distinctive experimental features. The intrinsic fluorescence of the cytochrome's porphyrin ring, rather than an extrinsic probe, was used. Orientational order was deduced from steady-state fluorescence excited by varying the incident evanescent polarization, as discussed in the theory of Thompson and Burghardt.[16] The TIR surface was quartz, coated with a thin film of the (semi)conductor SnO_2 connected via conducting glue and a wire to a variable-potential source, thereby forming an optically transparent electrode. The results indicate that the adsorbate's orientation can be affected by the imposed interfacial potential during the adsorption process, but once the adsorption has occurred, the orientations appear to become "locked in."

In a microscope, standard polarized epi-illumination cannot distinguish order from disorder in the polar direction (defined as the optical axis) because epi-illumination is polarized transverse to the optical axis and observation is along the optical axis at 180°. However, microscope TIR illumination can be partially polarized in the optical axis direction (the z-direction of Section 7.2) and can thereby detect order in the polar angle direction. Timbs and Thompson[102] used this feature to confirm that the popular lipid probe 3,3′-dioctadecylindocarbocyanine (diI) resides in a supported lipid monolayer with its dipoles parallel to the membrane surface, but labeled antibodies bound to the membrane exhibit totally random orientations.

7.5.4. Qualitative Observation of Labeled Cells

The most straightforward application of TIRF is to observe the location and (with time-lapse video) the motion of cell/substrate contacts. For this purpose, cells may be labeled by a membrane lipid fluorescent analogue such as diI (see Figure 7.9 and Refs. 5, 7, 41, and 103 for more photographic examples). For qualitative viewing, the TIRF contrast of the cell/substrate contacts over the background and cell autofluorescence is excellent in comparison to the contrast obtained with nonfluorescent techniques such as interference reflection contrast.[104, 105] Of course, labeling of cells can be cytotoxic, particularly under illumination. However, TIRF seems particularly advantageous for long-term viewing of cells compared to other fluorescence techniques, since the thin evanescent wave minimizes exposure of the cells' organelles to excitation light.

Quantitative determination of the absolute distance from the surface to a labeled cell membrane at a cell/substrate contact region can be based on the variation of $F(d)$ with θ.[106] This effort is challenging because corrections have to be made for θ-dependent reflection and transmission through four stratified layers (glass, culture medium, membrane, and cytoplasm), all with different refractive indices. For 3T3 cells, Lanni *et al.*[106] derived a plasma membrane/substrate spacing of 49 nm for focal contacts and 69 nm for "close" contacts elsewhere. They were also able to calculate an approximate refractive index for the cytoplasm of 1.358 to 1.374.

Another complication in the quantitation of TIRF on cells is the effect of the membrane thickness itself on the profile of the evanescent wave. Reichert and Truskey[105] have calculated that, in theory, the thickness of the membrane should have a negligible effect on the fluorescence and that a simplified theory of three stratified layers (glass/water/cytoplasm) should be adequate. The theory approximates for simplicity that scattering plays a negligible role and that fluorescence intensity versus angle of observation and fluorescence lifetime are not functions of distance to the interface z. Experiments that determine actual cell/substrate contact distances by an independent technique are now needed to confirm the validity of these convenient assumptions.

Evanescent light scattered by cells can be viewed directly, simply by removing the barrier filter. The contrast between cells and the background is rather low, and the scattered intensity is many orders of magnitude less than the evanescent wave intensity. On this qualitative basis, one might tentatively assume that scattering is not a significant factor. Nevertheless, at incidence angles very near the critical angle, the cells do cast a noticeable "shadow" along the surface.

In many cases of membrane labeling, some probe becomes internalized in living cells. Epi-illumination excites this internalized fluorescence from out-of focus planes and leads to a diffuse fluorescence that obscures detail. However, TIRF "optically sections" the sample, allowing observation of a distinct surface pattern even in the presence of a large amount of internalized label. The optical sectioning is particularly useful in viewing submembrane cytoplasmic filaments on thick cells. Although TIRF cannot view deeply into the cell as can confocal microscopy, it can display the submembrane filament structure with high contrast and sensitivity in the regions of cell/substrate contact.

A possible spatial correlation between submembrane filaments and surface acetylcholine receptors (AChR) on developing muscle cells in culture was investigated by Bloch *et al.*[107] Double labeling was used: a rhodamine-labeled second antibody for the cytoplasmic filaments, and fluorescein-labeled α-bungarotoxin for the AChR. Somewhat fortuitously for the use of TIR, the receptor clusters in this biological system happen to be found predominately in the general regions where the myotube plasma membrane is near the glass substrate, which allows TIR to effectively excite their fluorescence. Figure 7.13 shows double-labeled TIRF views of the relative distribution of AChR (labeled by fluorescein-labeled α-bungarotoxin) clustered on the surface of cultured rat myotubes and of certain specific non-AChR proteins (labeled by rhodamine-labeled antibodies) in or immediately under the membrane. The figure shows that AChR codistributes with 43K protein but interdigitates with vinculin. With standard epi-illumination on these intact thick cells, the cytoplasmic filament images would have been obscured by out-of-focus light.

One TIRF study found that some membrane proteins behave just oppositely to AChR: they avoid the cell/substrate contact regions.[108] When endothelial cells are grown on a bare glass surface or are brought into suspension, a specific membrane protein marked with antibodies appears all over the cell surface, as evidenced by epi-illumination and TIRF. However, when the cells are grown on (or returned to) a surface coated with their own extracellular matrix material, the protein disappears from the basal (cell/substrate-contacting) side of the cells.

The interaction between immune system cells and their targets often involves a specific and as yet incompletely understood surface reaction. This

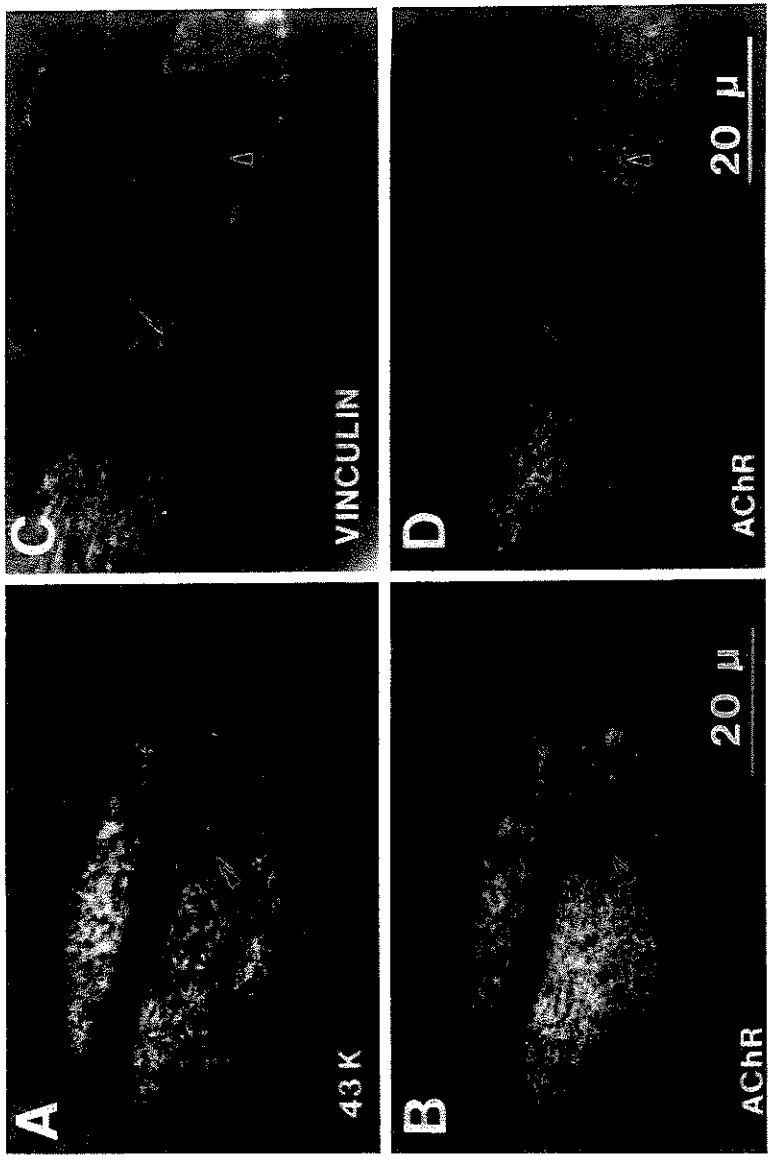

Figure 7.13. AChR clusters on a rat myotube in culture, visualized with (A) rhodamine anti-43K protein; (B) fluorescein-labeled α-bungarotoxin (corresponding field); (C) rhodamine-labeled anti-vinculin; and (D) fluorescein-labeled α-bungarotoxin (corresponding field). The antibodies were gifts from R. Bloch, University of Maryland Medical School. Note that AChR and 43K tend to aggregate in the same regions, whereas AChR and vinculin appear to exclude each other. Additional photographs are in Ref. 107.

interaction can be made optically accessible by modeling the target as a lipid monolayer or bilayer supported on glass.[53, 54] For example, Weis *et al.*[42] could visualize the contact region between basophils (which bear surface Fc receptors) and hapten-containing target model membranes by illuminating with TIR in the presence of fluoresceinated IgE antibodies. The contact region, where the Fc receptors are indirectly connected to the haptens through the IgE, appeared rather variegated and punctate, perhaps due to filopodia-like structures in the contact zone. This pattern could not be observed with conventional epi-fluorescence.

A variation of TIRF to observe cellular morphology, introduced by Gingell *et al.*,[109] produces essentially a negative of the standard fluorescence view of labeled cells. The solution surrounding the cells is doped with a non-adsorbing and nonpermeable fluorescent volume marker, fluorescein-labeled dextran. Focal contacts then appear as dark areas, and other areas appear brighter, depending on the depth of solution illuminated by the evanescent wave in the cell/substrate gap. A quantitative theory for converting fluorescence intensities into cell/substrate contact distances has been developed.[110] By using a high-refractive index glass ($n = 1.83$) as the TIR and cell substrate surface, a very shallow evanescent wave ($1/e$ decay distance ≈ 37 nm) can be produced[111] which minimizes the contribution from the cytoplasm and probes small undulations in the cell/substrate contact region.

7.5.5. Fluorescence Energy Transfer and TIRF

TIRF can be combined with fluorescence energy transfer to measure distances between fluorophores on a surface in the presence of a large background of bulk-dissolved fluorophores.

Burghardt and Axelrod[59] detected TIRF/energy transfer evidence of a change in the conformation of donor/acceptor-labeled bovine serum albumin upon the protein's adsorption to glass. In a TIRF/energy transfer study of relevance to cellular immunology, Watts *et al.*[112] explored whether helper T cells could force two nonidentical antigens in a target membrane into closer proximity with each other. These two antigens, one (a synthetic peptide) labeled with a fluorescence energy transfer donor and the other (a major histocompatibility complex) with an acceptor, were incorporated into a planar lipid bilayer on a TIR hydrophilic glass surface. Significant amount of the synthetic peptide remained in solution, so microscopic TIRF was needed to limit excitation to the region near the glass and overlaying lipid bilayer. TIRF also served to reduce the autofluorescence normally observed from the T cells that were allowed to settle on the lipid bilayer. It was found that fluorescence energy transfer occurred only in those microscopic lipid bilayer

regions where the T-cell surface came into close apposition with the bilayer. The conclusion was that the T-cell surface forces the two membrane antigens to which it binds to within a distance of 4 nm of each other.

7.5.6. Reaction Rates at Biosurfaces

Consider a labeled molecule in equilibrium between a surface-bound state and a free solute state:

$$\text{free solute} + \text{vacant surface site} \underset{k_2}{\overset{k_1}{\rightleftharpoons}} \text{surface-bound solute}$$

If the solute is fluorescent, the TIRF intensity (which is proportional to the concentration of surface-bound solute) can be monitored as a function of time to measure the binding kinetic rates k_1 and k_2. What is required is some sort of perturbation to disturb the equilibrium of the fluorescent species.

Using a concentration jump as the perturbation, Sutherland *et al.*[113] measured the kinetics of binding of fluorescein-labeled human IgG (present as an antigen in solution) to surface-immobilized sheep anti-human IgG. Two TIRF surfaces were used: a planar slide and a fiber-optic cylinder. Also using a TIRF recovery after a concentration jump, Kalb *et al.*[114] measured the slow ($\sim 10^{-4}\,s^{-1}$) unbinding kinetics of anti-trinitrophenol (TNP) antibodies in solution and a TNP-derivatized lipid in a planar bilayer.

To increase the speed of the TIRF-based kinetic techniques, the perturbation can be optical rather than chemical. If the evanescent wave intensity is briefly flashed brightly, then some of the fluorophores associated with the surface will be photobleached. Subsequent exchange with unbleached dissolved fluorophores in equilibrium with the surface will lead to a recovery of fluorescence, excited by a continuous but much attenuated evanescent wave. The time course of this recovery is a measure of the desorption kinetic rate k_2. This technique[115] is called TIR/FRAP (or TIR/FPR) in reference to fluorescence recovery after photobleaching (or fluorescence photobleaching recovery).

Adsorption kinetics are especially interesting when compared with surface diffusion rates of the adsorbate. This is because of the theoretical possibility that nonspecific and reversible adsorption of a ligand (say, a hormone), followed by two-dimensional diffusion on the membrane, may enhance the reaction rate with a specific binding patch (say, a hormone receptor).[116, 117] A similar effect might enhance the reaction rates between a surface-immobilized enzyme and bulk-dissolved substrate, thereby speeding some reactions in industrial chemistry.

TIR/FRAP can be used to measure both surface diffusion coefficients and on/off kinetic rates, if the evanescent wave intensity is variegated over a distance on the surface that is short compared to the characteristic distance covered by surface diffusion within the time available before desorption.[115] Several studies have utilized TIR/FRAP in this manner. The adsorption-/desorption kinetics and surface diffusion of rhodamine-labeled bovine serum albumin (BSA) at a glass surface have been examined using a TIR illumination area focused into a thin line.[58] BSA was found to adsorb with a wide range of reversible kinetic rates, with more than half of the adsorption being reversible at higher bulk concentrations ($> \sim 1$ mg/ml). About 20% of the adsorbed BSA could surface diffuse, with a coefficient of about 5×10^{-9} cm^2/sec. This is fast enough to carry a BSA molecule at least $\sim 1\,\mu$m on the average before it desorbs within 4 sec.

These results were extended by Tilton *et al.*[118] to adsorption of eosin-labeled BSA on polymer surfaces. They also found a component that surface diffuses, with coefficients ranging from 1.2×10^{-9} to 2.6×10^{-9} cm^2/s, depending on surface type. In this study, intersecting TIR laser beams rather than a focused stripe were used to define the spatial intensity variation. Surface diffusion was even noted for the most irreversibly adsorbed eosin-labeled BSA components; this was evident on samples rinsed for long periods with unlabeled BSA after exposure to eosin-labeled BSA. The surface diffusion coefficient of the irreversibly bound BSA was found to be a strong function of adsorbed concentration.[119]

A wide range of reversible adsorption kinetic rates was also found by TIR/FRAP for another protein, lysozyme, on a substrate with a different surface charge, alkylated silicon oxide.[61] It is possible that the wide range of rates results from a spectrum of surface binding site types and/or formation of multilayers of adsorbed protein.

A preliminary TIR/FRAP report[120] gives the desorption rate (k_2) for binding of prothrombin, a key protein in surface-activated thrombogenesis, with acidic (phosphatidylserine-containing) supported phospholipid bilayers. Another[121] gives desorption rates for specific binding between Fab antibody fragments and a lipid–hapten in a planar membrane. Knowledge of the desorption rates for such specific binding not only tells us how much time a bound pair have available to engage in more surface reactions together, but also allows us to calculate (with quantitative knowledge of the equilibrium binding constant) the specific adsorption rate (k_1). If (as in this Fab/lipid–hapten case) k_1 is calculated to be less than its theoretical diffusion-limited value, then one can conclude that the reaction is not diffusion-limited; that is, not every encounter leads to a successful binding event.

For TIR/FRAP to be useful for chemical kinetics studies on intact biological membranes as opposed to reconstituted or artificial surfaces, two problems must be confronted: (1) how to position the membrane in a TIR

system; and (2) how to overcome background binding to the substrate to which the membrane is attached.

Proper positioning requires that at least part of the membrane be in the evanescent wave and that the surface under study (external or cytoplasmic) be accessible to chemical exchange with the bulk. This positioning has been successfully accomplished with erythrocyte ghosts.[122] After the glass substrate is covalently coated with poly-L-lysine, erythrocytes are allowed to adhere, followed by hyposmotic shock. Rather than floating away or crumpling up on the surface, the membrane ghosts flatten into circular disks on the glass with a characteristic tear that exposes the outer surface and the cytoplasmic surface to the solution in their own distinct regions (Figure 7.14). This technique or a modification of it may also work for other cell types.

This flattened erythrocyte preparation has been used to study reversible nonspecific adsorption kinetics and surface diffusion of insulin on the external surface of erythrocytes.[123] The nonspecific adsorption of insulin to the polylysine-coated substrate is very large compared to the adsorption to the flattened membrane adhered to the substrate. Fortunately, this nonspecific background fluorescence can be very successfully quenched simply by preparing the polylysine coating on an aluminum-film-coated glass surface, rather than on bare glass. As discussed in Section 7.3, the aluminum abolishes the fluorescence of fluorophores adsorbed directly onto the polylysine substrate, but the fluorophores adsorbed to the erythrocyte surface are not substantially quenched, because they are spaced at least two membrane thicknesses away.

The results of this TIR/FRAP study are that $\sim 80\%$ of the nonspecific binding of fluorescein-labeled insulin to the external face of red cell membranes is reversible within < 100 s, and the mean residency time of the reversibly adsorbed insulin ranges from ~ 0.4 s to ~ 20 s. Surface diffusion of nonspecifically adsorbed insulin (as investigated by an TIR intersecting beam interference fringe pattern; see Figure 7.5) was immeasurably small: it is insufficient to carry a typical insulin more than $\sim 0.3\ \mu$m before desorption.

At some point, these kinetic results for insulin on a biological membrane should be compared to kinetic results for insulin on an artificial lipid membrane, when such results become available. This comparison should be especially interesting in view of the suggestion by Sui *et al.*[124] that nonspecific equilibrium binding of insulin to planar membranes is a function not only of membrane charge but also of some sort of nonelectrostatic mechanism, based on their TIRF experiments with a chamber adapted to a standard spectrofluorimeter chamber.

Another TIR/FRAP study on biological cell membranes has examined the reversible but specific binding kinetics of fluorescence-labeled epidermal growth factor to the surface of cells.[125] The background problem here was solved simply by choosing cells with a very large concentration of epidermal

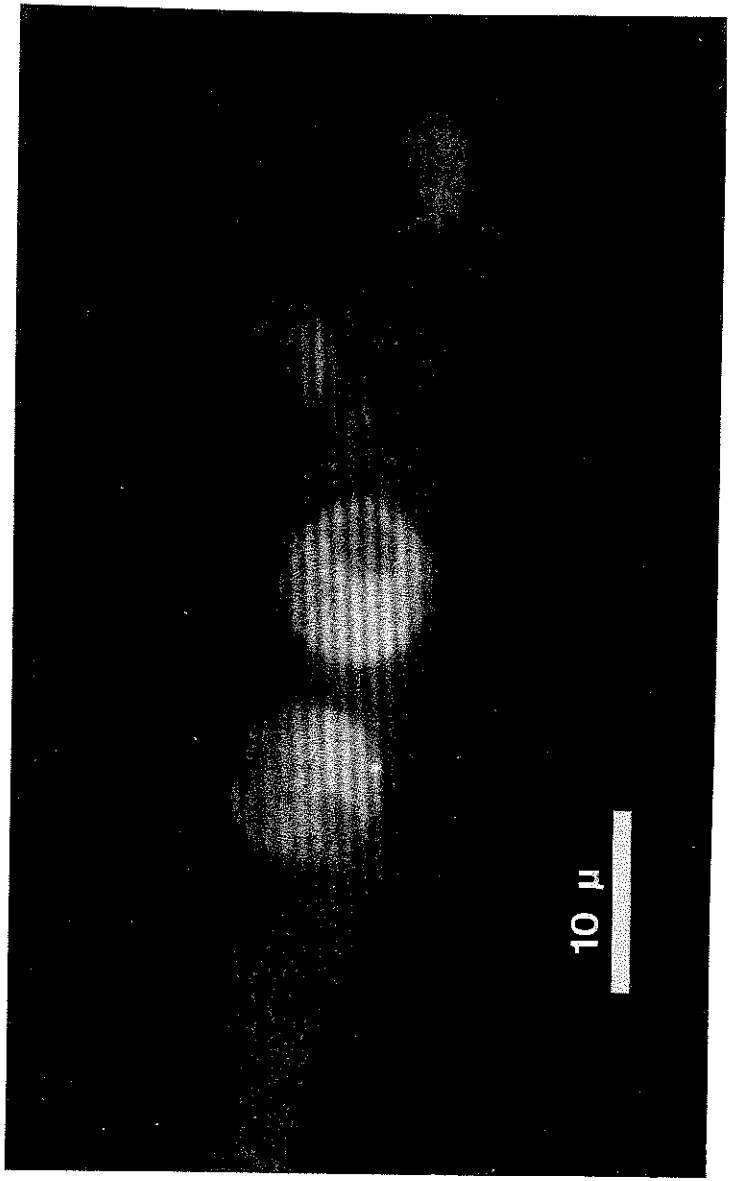

Figure 7.14. Erythrocyte ghosts adhered to aluminum film-coated glass covalently coated with polylysine. The TIR fluorescence is due to adsorbed fluorescein-labeled insulin; the background (off-cells) is dark only because of metal surface quenching. The small, darker circular regions in each ghost are open tears in the apical membrane which expose the cytoplasmic face of the basal membrane; this can be shown in other experiments by use of lipid, lectin, and cytoplasmic filament-specific labels. The stripes are due to interfering incident TIR laser beams, produced by the optical configuration shown in Figure 7.15.

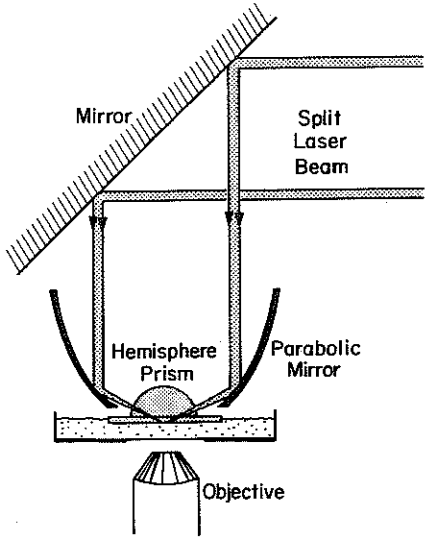

Figure 7.15. Intersecting TIR beams split from the same laser to produce interference fringes for viewing in an inverted microscope, as used for Figure 7.14. The beams reflect off the parabolic mirror and then propagate radially into a hemispherical prism. The drawing shows the beams intersecting at 180° for pictorial clarity only; for the photograph of Figure 7.14, the beams strike the parabolic mirror at adjustable nearby points and thereby intersect at an adjustable relative angle ϕ of ~20°. The TIR surface, at a glass slide surface just below the prism, is positioned at the focus of the parabola.

growth factor (EGF) receptors: the A431 human epidermoid cell line. No special procedures were used to flatten the cells; cell/substrate contact regions that were accessible enough to be labeled by EGF were observed. More than 85% of the EGF binds reversibly, with a range of characteristic times from ~20 s to ~250 s. Various control experiments and theoretical arguments show that the fluorescence recovery after photobleaching was indeed due to on/off kinetics of EGF binding to its receptors, and not to diffusion of the EGF receptors themselves, nor to restricted-access bulk diffusion of EGF to the membrane regions in the evanescent wave.

Given the recent successes in using TIRF to detect weak but specific equilibrium binding to surfaces, we can expect more results on the kinetics of such binding in the near future. Because of the close connection between chemical kinetics and dynamical processes in biology, TIR/FRAP measurements undoubtedly will be expanded to study reversible specific binding kinetic rates between a variety of soluble ligands and their cell surface receptors in natural or reconstituted biological membranes; the nonspecific but biologically important binding between cytoplasmic filaments and lipids in supported bilayer systems; and the attachment/detachment rates of cytoplasmic filaments with protein anchors in biological membranes..

7.5.7. TIRF Combined with Fluorescence Correlation Spectroscopy (FCS)

The volume defined by the depth of the evanescent wave in the area defined by the image plane diaphragm of a microscope can be extremely

small, down to about 0.01 μm^3. Within this volume, the entrance or exit of a single fluorophore can cause a significant change in the fluorescence intensity. In fact, these TIRF fluctuations are clearly visible to the "naked eye" through the microscope. By autocorrelating (on-line) the random noise arising from such statistical fluctuations (a technique called fluorescence correlation spectroscopy, or FCS), one can obtain information about three parameters: the mean time of surface binding ($=1/k_2$), the surface diffusion coefficient, and the absolute mean number of fluorescent molecules bound per surface area (without requiring any information about quantum efficiencies or light collection efficiencies).

Two investigations have combined TIR with FCS thus far. The first[126] adapted TIR/FCS to measure the absolute concentration of virions in solution. The other[127] measured the adsorption/desorption kinetics of immunoglobulin on a protein-coated surface on the millisecond time scale.

Although TIR/FCS and TIR/FRAP both give similar information about kinetic rates and surface diffusion, and the mathematics of the two is similar,[115] there is an interesting and perhaps useful difference. Thompson[128] has shown theoretically that with TIR/FCS, but not with TIR/FRAP, one can infer kinetic rates of a nonfluorescent species as it competes with fluorescent species for the same nearly saturated surface sites.

7.6. Summary and Comparisons

TIRF is an experimentally simple technique for selective excitation of fluorophores on or near a surface. It can be set up on a standard upright or inverted microscope, preferably but not necessarily with a laser source, or in a nonmicroscopic custom setup or commercial spectrofluorimeter. In a microscope, the TIRF setup is compatible and rapidly interchangeable with bright-field, dark-field, phase contrast, and epi-illumination and accommodates a wide variety of common microscope objectives without alteration.

Confocal microscopy (CM) is another microscope technique for apparent optical sectioning, achieved by exclusion of out-of-focus emitted light with a set of image plane pinholes. CM has the clear advantage in versatility; its method of optical sectioning works at any plane of the sample, not just at an interface between substances having dissimilar refractive indices. However, other differences exist which, in some special applications, can favor the use of TIRF:

(a) The depth of the optical section in TIRF is ~0.1 μm whereas in CM it is relatively thick, ~0.6 μm.
(b) In some applications (e.g., FRAP, FCS, or on cells whose viability is damaged by light), illumination, not just detected emission, is best restricted to a thin section; this is possible only with TIRF.

(c) Since the TIRF setup can be adapted to and made interchangeable with existing standard microscope optics, even with "homemade" components, it is much less expensive than CM.
(d) TIRF has much better light throughput than currently available confocal microscopes.

Cell/substrate contacts can be located by a nonfluorescence technique completely distinct from TIRF, known as "internal reflection microscopy" (IRM).[129] Using conventional illumination sources, IRM visualizes cell/substrate contacts as dark regions. IRM has the advantage that it does not require the cells to be labeled, but the disadvantages that it contains no information about biochemical specificities in the contact regions and that it is less sensitive to changes in contact distance (relative to TIRF) within the critical first 100 nm from the surface.

Applications of TIRF in cell biology and surface chemistry include:

1. Localization of cell/substrate contact regions in cell culture.
2. High-contrast visualization of submembrane cytoskeletal structure on thick cells.
3. Measurement of the kinetic rates and surface diffusion of reversibly bound biomolecules at flattened biological and model membrane surfaces and at specifically derivatized glass surfaces (e.g., with immobilized enzymes).
4. Measurement of the concentration and orientational distributions of fluorescent molecules as a function of distance from the surface.
5. Measurement of intermolecular distances between fluorescent surface-bound molecules in the presence of a large excess of fluorophore or background fluorescence in the bulk.
6. Reduction of cell autofluorescence relative to fluorescence excited at cell/substrate contacts.
7. Construction of waveguide or optical-fiber fluorosensors usable for medical diagnoses.

Acknowledgments

We thank Dr. Nancy L. Thompson for helpful discussions and Dr. Marisela Velez, Ariane McKiernan, Andrea Stout, and Dong Wang of our lab for their contributions to various aspects of TIRF discussed here. This work was supported by a USPHS NIH grant NS 14565 and NSF grant DMB 8805296.

References

1. T. Hirschfeld, Total reflection fluorescence, *Can. Spectrosc. 10*, 128 (1965).
2. N. J. Harrick and G. I. Loeb, Multiple internal reflection spectrometry, *Anal. Chem. 45*, 687–691 (1973).
3. M. N. Kronick and W. A. Little, A new immunoassay based on fluorescence excitation by internal reflection spectroscopy, *J. Immunol. Methods 8*, 235–240 (1975).
4. R. W. Watkins and C. R. Robertson, A total internal reflection technique for the examination of protein adsorption, *J. Biomed. Mater. Res. 11*, 915–938 (1977).
5. D. Axelrod, T. P. Burghardt, and N. L. Thompson, Total internal reflection fluorescence, *Annu. Rev. Biophys. Bioeng. 13*, 247–268 (1984).
6. E. H. Hellen, R. M. Fulbright, and D. Axelrod, Total internal reflection fluorescence: Theory and applications at biosurfaces, in: *Spectroscopic Membrane Probes* (L. M. Loew, ed.), Vol. II, pp. 47–49, CRC Press, Boca Raton, Florida (1988).
7. D. Axelrod, Total internal reflection fluorescence at biological surfaces, in: *Noninvasive Techniques in Cell Biology* (J. K. Foskett and S. Grinstein, eds.), pp. 93–127, Wiley-Liss, New York (1990).
8. T. P. Burghardt and N. L. Thompson, Evanescent intensity of a focused Gaussian light beam undergoing total internal reflection in a prism, *Opt. Eng. 23*, 62–67 (1984).
9. H. Chew, D. Wang, and M. Kerker, Elastic scattering of evanescent electromagnetic waves, *Appl. Opt. 18*, 2679–2687 (1979).
10. M. Born and E. Wolf, *Principles of Optics*, 5th ed., Pergamon Press, Oxford (1975).
11. H. J. Simon, D. E. Mitchell, and J. G. Watson, Surface plasmons in silver film. A novel undergraduate experiment, *Am. J. Phys. 43*, 630–636 (1975).
12. G. W. Ford and W. H. Weber, Electromagnetic interactions of molecules with metal surfaces, *Phys. Rep. 113*, 195–287 (1984).
13. W. H. Weber and C. F. Eagen, Energy transfer from an excited dye molecule to the surface plasmons of an adjacent metal, *Opt. Lett. 4*, 236–238 (1979).
14. W. Lukosz and R. E. Kunz, Fluorescence lifetime of magnetic and electric dipoles near a dielectric surface, *Opt. Commun. 20*, 195–199 (1977).
15. W. Lukosz and R. E. Kunz, Light emission by magnetic and electric dipoles close to a plane interface. I. Total radiated power, *J. Opt. Soc. Am. 67*, 1607–1614 (1977).
16. N. L. Thompson and T. P. Burghardt, Total internal reflection fluorescence: Measurement of spatial and orientation distributions of fluorophores near planar dielectric interfaces, *Biophys. Chem. 25*, 91–97 (1986).
17. W. Lukosz and R. E. Kunz, Light emission by magnetic and electric dipoles close to a plane interface. II. Radiation patterns of perpendicularly oriented dipoles, *J. Opt. Soc. Am. 67*, 1615–1619 (1977).
18. C. K. Carniglia, L. Mandel, and K. H. Drexhage, Absorption and emission of evanescent photons, *J. Opt. Soc. Am. 62*, 479–486 (1972).
19. E.-H. Lee, R. E. Benner, J. B. Fen, and R. K. Chang, Angular distribution of fluorescence from liquids and monodispersed spheres by evanescent wave excitation, *Appl. Opt. 18*, 862–868 (1979).
20. T. P. Burghardt and N. L. Thompson, Effect of planar dielectric interfaces on fluorescence emission and detection: Evanescent excitation with high aperture collection, *Biophys. J. 46*, 729–737 (1984).
21. N. L. Thompson, H. M. McConnell, and T. P. Burghardt, Order in supported phospholipid monolayers detected by dichroism of fluorescence excited with polarized evanescent illumination, *Biophys. J. 46*, 739–747 (1984).
22. R. R. Chance, A. Prock, and R. Silbey, Molecular fluorescence and energy transfer near interfaces, *Adv. Chem. Phys. 37*, 1–65 (1978).

23. R. R. Chance, A. Prock, and R. Silbey, Comments on the classical theory of energy transfer, *J. Chem. Phys. 62*, 2245–2253 (1975).
24. K. H. Drexhage, Interaction of light with monomolecular dye lasers, *Prog. Opt. 12*, 163–232 (1974).
25. K. H. Drexhage, Influence of a dielectric interface on fluorescence decay time, *J. Lumin. 12*, 693–701 (1970).
26. C. F. Eagen, W. H. Weber, S. L. McCarthy, and R. W. Terhune, Time dependent decay of surface plasmon-coupled molecular fluorescence, *Chem. Phys. Lett. 75*, 274–277 (1980).
27. H. Kuhn, Classical aspects of energy transfer in molecular systems, *J. Chem. Phys. 53*, 101–108 (1970).
28. M. R. Philpott, Effect of surface plasmons on transitions in molecules, *J. Chem. Phys. 62*, 1812–1817 (1975).
29. T. Tamir, J. J. Burke, and G. I. Stegeman, Surface polariton-like waves guided in thin, lossy metal films, *Phys. Rev. B 33*, 5186–5201 (1986).
30. B. N. J. Persson, Theory of the damping of excited molecules located above a metal surface, *J. Phys. C 11*, 4251–4269 (1978).
31. W. H. Weber and G. W. Ford, Enhanced Raman scattering by adsorbates including the nonlocal response of the metal and excitation of nonradiative modes, *Phys. Rev. Lett. 44*, 1774–1777 (1980).
32. P. Ye and Y. R. Shen, Local field effect on linear and nonlinear optical properties of adsorbed molecules, *Phys. Rev. B 28*, 4288–4294 (1983).
33. E. H. Hellen and D. Axelrod, Fluorescence emission at dielectric and metal-film interfaces, *J. Opt. Soc. Am. B 4*, 337–350 (1987).
34. V. Hlady, R. A. VanWagenen, and J. D. Andrade, Total internal reflection intrinsic fluorescence (TIRIF) spectroscopy applied to protein adsorption, in: *Protein Adsorption* (J. D. Andrade, ed.), *Interfacial Aspects of Biomedical Polymers*, Vol. 2, Chapter 2, Plenum Press, New York (1985).
35. V. Hlady, D. R. Reinecke, and J. D. Andrade, Fluorescence of adsorbed protein layers: I. Quantitation of total internal reflection fluorescence, *J. Colloid Interface Sci. 111*, 555–569 (1986).
36. S. A. Rockhold, R. D. Quinn, R. A. VanWegenen, J. D. Andrade, and M. Reichert, Total internal reflection fluorescence (TIRF) as a quantitative probe of protein adsorption, *J. Electroanal. Chem. 150*, 261–275 (1983).
37. C. Allain, D. Ausserre, and F. Rondelez, Direct optical observation of interfacial depletion layers in polymer solutions, *Phys. Rev. Lett. 49*, 1694–1697 (1982).
38. D. Ausserre, H. Hervet, and F. Rondelez, Concentration profile of polymer solutions near a solid wall, *Phys. Rev. Lett. 54*, 1948–1951 (1985).
39. F. Rondelez, D. Ausserre, and H. Hervet, Experimental studies of polymer concentration profiles at solid–liquid and liquid–gas interfaces by optical and X-ray evanescent wave techniques, *Annu. Rev. Phys. Chem. 38*, 317–347 (1987).
40. M. Nakache, A. B. Schreiber, H. Gaub, and H. M. McConnell, Heterogeneity of membrane phospholipi in endothelial cells depends on cell substrate, *Nature 317*, 75–77 (1985).
41. D. Axelrod, Total internal reflection fluorescence microscopy, in: *Fluorescence Microscopy of Living Cells in Culture B* (D. L. Taylor and Y.-L. Wang, eds.), *Methods in Cell Biology*, Vol. 30, pp. 245–270, Academic Press, San Diego, California (1989).
42. R. M. Weis, K. Balakrishnan, B. A. Smith, and H. M. McConnell, Stimulation of fluorescence in a small contact region between rat basophil leukemia cells and planar lipid membrane targets by coherent evanescent radiation. *J. Biol. Chem. 257*, 6440–6445 (1982).
43. A. L. Stout and D. Axelrod, Evanescent field excitation of fluorescence by epi-illumination microscopy, *Appl. Opt. 28*, 5237–5242 (1989).
44. J. A. Bloom and W. W. Webb, Photodamage to intact erythrocyte membranes at high laser intensities; methods of assay and suppression, *J. Histochem. Cytochem. 32*, 608–616 (1984).

45. G. Bock, M. Hilchenbach, K. Schaenstein, and G. Wick, Photometric analysis of antifading reagents for immunofluorescence with laser and conventional illumination sources, *J. Histochem. Cytochem. 33*, 699–705 (1985).
46. G. D. Johnson and G. M. deC. Noguerira Araujo, A simple method of reducing the fading of immunofluorescence during microscopy, *J. Immunol. Methods 43*, 349–350 (1981).
47. G. L. Picciolo and D. S. Kaplan, Reduction of fading of fluorescent reaction product for microphotometric quantitation, *Adv. Appl. Microbiol. 30*, 197–324 (1984).
48. H. Storz, Investigations of fading of immunofluorescence objects, *Acta Histochem. (Jena) 71*, 2–9 (1982).
49. J. C. White and L. Stryer, Photostability studies of phycobiliprotein fluorescent labels, *Anal. Biochem. 161*, 442–452 (1987).
50. B. S. Jacobson, J. Cronin, and D. Branton, Coupling polylysine to glass beads for plasma membrane isolation, *Biochim. Biophys. Acta 506*, 81–96 (1978).
51. V. VonTscharner and H. M. McConnell, Physical properties of lipid monolayers on alkylated planar glass surfaces, *Biophys. J. 36*, 421–427 (1981).
52. H. M. McConnell, T. H. Watts, R. M. Weis, and A. A. Brian, Supported planar membranes in studies of cell–cell recognition in the immune system, *Biochim. Biophys. Acta 864*, 95–106 (1986).
53. N. L. Thompson and A. G. Palmer, Model cell membranes on planar substrates, *Commun. Mol. Cell. Biophys. 5*, 39–56 (1988).
54. N. L. Thompson, A. G. Palmer, L. L. Wright, and P. E. Scarborough, Fluorescence techniques for supported planar model membranes, *Commun. Mol. Cell. Biophys. 5*, 109–113 (1988).
55. V. Hlady and J. D. Andrade, Fluorescence emission from adsorbed bovine albumin and albumin-bound 1-anilinonaphthalene-8-sulfonate studied by TIRF, *Colloids Surf. 32*, 359–368 (1988).
56. C.-G. Gölander, V. Hlady, K. Caldwell, and J. D. Andrade, Absorption of human lysozyme and adsorbate enzyme activity as quantified by means of total internal reflection fluorescence, ^{125}I labeling and ESCA, *Colloids Surf. 50*, 113–130 (1990).
57. R. M. Zimmermann, C. F. Schmidt, and H. E. Gaub, Absolute quantities and equilibrium kinetics of macromolecular adsorption measured by fluorescence photobleaching in total internal reflection, *J. Colloid Interface Sci. 139*, 268–280 (1990).
58. T. P. Burghardt and D. Axelrod, Total internal reflection/fluorescence photobleaching recovery study of serum albumin adsorption dynamics, *Biophys. J. 33*, 455–468 (1981).
59. T. P. Burghardt and D. Axelrod, Total internal reflection fluorescence study of energy transfer in surface-adsorbed and dissolved bovine serum albumin, *Biochemistry 22*, 979–985 (1983).
60. V. Hlady and J. D. Andrade, A TIRF titration study of 1-anilinonaphthalene-8-sulfonate binding to silica-adsorbed bovine serum albumin, *Colloids Surf. 42*, 85–96 (1989).
61. C. F. Schmidt, R. M. Zimmermann, and H. E. Gaub, Multilayer adsorption of lysozyme on a hydrophobic substrate, *Biophys. J. 57*, 577–588 (1990).
62. M. R. Rainbow, S. Arterton, and R. C. Eberhardt, Fluorescence lifetime measurements using total internal reflection fluorimetry: Evidence for a conformational change adsorbed to quartz, *J. Biomed. Mater. Res. 21*, 539–555 (1987).
63. H. Bader, R. VanWagenen, J. D. Andrade, and H. Ringsdorf, Interactions of concanavalin A with polymerized monolayers, *J. Colloid Interface Sci. 101*, 246–249 (1984).
64. G. K. Iwamoto, L. C. Winterton, R. S. Soker, R. A. VanWagenen, J. D. Andrade, and D. F. Mosher, Fibronectin adsorption detected by interfacial fluorescence, *J. Colloid Interface Sci. 106*, 459–463 (1985).
65. R. Lowe, V. Hlady, J. D. Andrade, and R. A. VanWagenen, Human haptoglobin adsorption by a total internal reflection fluorescence method, *Biomaterials 7*, 41–44 (1986).
66. V. Hlady, J. Rickel, and J. D. Andrade, Fluorescence of adsorbed protein layers. II. Adsorp-

tion of human lipoproteins studies by total internal reflection intrinsic fluorescence, *Colloids Surf. 34*, 171–183 (1988).
67. D. Horsley, J. Herron, V. Hlady, and J. D. Andrade, Human and hen lysozyme adsorption: A comparative study using total internal reflection fluorescence spectroscopy and molecular graphics, in: *Proteins at Interfaces: Physicochemical and Biochemical Studies* (J. L. Brash and T. A. Horbett, eds.), ACS Symposium Series No. 343, pp. 290–305, American Chemical Society, Washington, D.C. (1987).
68. V. Hlady, D. R. Reinecke, and J. D. Andrade, Fluorescence of adsorbed protein layers: Quantitation of total internal reflection fluorescence, *J. Colloid Interface Sci. 111*, 555–569 (1986).
69. K. Newby, W. M. Reichert, J. D. Andrade, and R. E. Benner, Remote spectroscopic sensing of chemical adsorption using a single multimode optical fiber, *Appl. Opt. 23*, 1812–1814 (1984).
70. J. D. Andrade, W. M. Reichert, D. E. Gregonis, and R. A. VanWagenen, Remote fiber-optic biosensors based on evanescent-excited fluoro-immunoassay: Concept and progress, *IEEE Trans. Electron Devices ED-32*, 1175–1179 (1985).
71. K. Newby, J. D. Andrade, R. E. Benner, and W. M. Reichert, Remote sensing of protein adsorption using a single optical fiber, *J. Colloid Interface Sci. 111*, 280–282 (1986).
72. C. Dahne, R. M. Sutherland, J. F. Place, and A. S. Ringrose, Detection of antibody–antigen reactions at a glass–liquid interface: A novel fibre-optic sensor concept, *Conf. Proc. OFS '84, 2nd International Conference on Optical Fiber Sensors*, pp. 75–79 (1984).
73. I. J. Higgins, W. G. Potter, and A. P. F. Turner, Opto-electronic immunosensors: A review of optical immunoassay at continuous surfaces, *Biosensors 1*, 321–353 (1985).
74. W. M. Reichert, J. T. Ives, P. A. Suci, and V. Hlady, Excitation of fluorescent emission from solutions at the surface of polymer thin-film waveguides: An integrated optics technique for the sensing of fluorescence at the polymer/solution interface, *Appl. Spectrosc. 41*, 636–639 (1987).
75. S. Zhao and W. M. Reichert, Protein adsorption using an evanescent chemical sensor with a fused optical fiber coupler, *J. Colloid Interface Sci. 140*, 294–297 (1990).
76. J. T. Ives and W. M. Reichert, Protein adsorption on the surface of a thin-film polymer integrated optical waveguide, *Appl. Spectrosc. 42*, 68–72 (1988).
77. T. R. Glass, S. Lackie, and T. Hirschfeld, Effect of numerical aperture on signal level in cylindrical waveguide evanescent fluorosensors, *Appl. Opt. 26*, 1218–1287 (1987).
78. K. R. Rogers, J. J. Valdes, and E. Eldefrawi, Acetylcholine receptor fiber-optic evanescent fluorosensor, *Anal. Biochem. 182*, 353–359 (1989).
79. V. Hlady, J. N. Lin, and J. D. Andrade, Spatially resolved detection of antibody–antigen reaction on solid/liquid interface using total internal reflection excited antigen fluorescence and charge-coupled device detection, *Biosensors Bioelectronics 5*, 291–301 (1990).
80. K. C. Hartner, J. W. Carr, and J. M. Harris, Total internal reflection fluorescence for adsorbed probe molecule studies of liquid/solid interfacial environments, *Appl. Spectrosc. 43*, 81–86 (1989).
81. T. Nakashima and A. Fujishima, Highly sensitive analysis of SnO_2/solution interface by internal reflection-fluorescence spectroscopy, *Chem. Lett. 1990* (11), 1995–1998.
82. V. Hlady, C. Golander, and J. D. Andrade, Hydrophobicity gradient on silica surfaces: A study using total internal reflection fluorescence spectroscopy, *Colloids Surf. 33*, 185–190 (1988).
83. S. W. Tendian, N. L. Thompson, and B. R. Lentz, Calcium-independent binding of prothrombin to negatively charged membranes, *Biophys. J. 57*, 72a (1990).
84. C. L. Poglitsch and N. L. Thompson, Interaction of antibodies with Fc receptors in substrate-supported planar membranes measured by total internal reflection fluorescence microscopy, *Biochemistry 29*, 248–254 (1990).

85. C. L. Poglitsch and N. L. Thompson, Substrate-supported planar membranes containing murine antibody Fc receptors: A total internal reflection fluorescence microscopy study, in: *Biosensor Technology, Fundamentals and Applications* (R. P. Buck, W. E. Hatfield, M. Umañia, and E. F. Bowden, eds.), pp. 375–382, Marcel Dekker, New York (1990).
86. M. L. Pisarchick and N. L. Thompson, Binding of a monoclonal antibody and its Fab fragment to supported phospholipid monolayers measured by total internal reflection fluorescence microscopy, *Biophys. J. 58*, 1235–1239 (1990).
87. F. Rondelez, D. Ausserre, and H. Hervet, Experimental studies of polymer concentration profiles at solid–liquid and liquid–gas interfaces by optical and X-ray evanescent wave techniques, *Annu. Rev. Phys. Chem. 38*, 317–347 (1987).
88. W. M. Reichert, J. T. Suci, J. T. Ives, and J. D. Andrade, Evanescent detection of adsorbed protein concentration–distance profiles: Fit of simple models to variable-angle total internal reflection fluorescence data, *Appl. Spectrosc. 41*, 503–507 (1987).
89. P. A. Suci and W. M. Reichert, Determination of fluorescence density profiles of Langmuir–Blodgett deposited films using standing light waves, *Langmuir 4*, 1131–1141 (1988).
90. C. Allain, D. Ausserre, and F. Rondelez, Direct optical observation of interfacial depletion layers in polymer solutions, *Phys. Rev. Lett. 49*, 1694–1697 (1982).
91. D. Ausserre, H. Hervet, and F. Rondelez, Concentration profile of polymer solutions near a solid wall, *Phys. Rev. Lett. 54*, 1948–1951 (1985).
92. A. Kurahashi, A. Itaya, H. Masuhara, M. Sato, T. Yamada, and C. Koto, Depth distribution of fluorescent species in silk fabrics as revealed by total internal reflection fluorescence microscopy, *Chem. Lett. 1986*, 1413–1416.
93. A. I. Mahan and C. V. Bitterli, Total internal reflection: A deeper look, *Appl. Opt. 17*, 509–519 (1978).
94. T. P. Burghardt, Polarized fluorescent emission from probes near dielectric surfaces, *Chem. Phys. Lipids 50*, 271–287 (1989).
95. P. Suci and V. Hlady, Fluorescence lifetime components of Texas Red-labeled bovine serum albumin: Comparison of bulk and adsorbed states, *Colloids Surf. 51*, 89–104 (1990).
96. M. Masuhara, S. Tazuke, N. Tamai, and I. Yamazaki, Time-resolved total internal reflection fluorescence spectroscopy for surface photophysics studies, *J. Phys. Chem. 90*, 5830–5835 (1986).
97. A. Itaya, T. Yamada, K. Tokuda, and H. Masuhara, Interfacial characteristics of poly(methyl methacrylate) film: Aggregation of pyrene and micropolarity revealed by time-resolved total internal reflection fluorescence spectroscopy, *Polym. J. 22*, 697–704 (1990).
98. H. Fukumura and K. Hayashi, Time-resolved fluorescence anisotropy of labeled plasma proteins adsorbed to polymer surfaces, *J. Colloid Interface Sci. 135*, 435–442 (1990).
99. A. Itaya, A. Kurahashi, H. Masuhara, N. Tamai, and I. Yamazaki, Dynamic fluorescence microprobe method utilizing total internal reflection phenomena, *Chem. Lett. 1987*, 1079–1082.
100. L. E. Morrison and G. Weber, Biological membrane modeling with a liquid/liquid interface. Probing mobility and environment with total internal reflection excited fluorescence, *Biophys. J. 52*, 367–379 (1987).
101. J. G. E. M. Fraaije, J. M. Kleijn, M. van der Graaf, and J. C. Dijt, Orientation of adsorbed cytochrome c as a function of the electrical potential of the interface studied by total internal reflection fluorescence, *Biophys. J. 57*, 965–975 (1990).
102. M. M. Timbs and N. L. Thompson, Slow rotational mobilities of antibodies and lipids associated with substrate-supported phospholipid monolayers as measured by polarized fluorescence photobleaching recovery, *Biophys. J. 58*, 413–428 (1990).
103. D. Axelrod, Cell–substrate contacts illuminated by total internal reflection fluorescence, *J. Cell Biol. 89*, 141–145 (1981).

104. J. Bailey and D. Gingell, Contacts of chick fibroblasts on glass: Results and limitations of quantitative interferometry, *J. Cell Sci. 90*, 215–224 (1988).
105. W. M. Reichert and G. A. Truskey, Total internal reflection fluorescence (TIRF) microscopy. I. Modeling cell contact region fluorescence, *J. Cell Sci. 96*, 219–230 (1990).
106. F. Lanni, A. S. Waggoner, and D. L. Taylor, Structural organization of interphase 3T3 fibroblasts studied by total internal reflection fluorescence microscopy, *J. Cell Biol. 100*, 1091–1102 (1985).
107. R. J. Bloch, M. Velez, J. Krikorian, and D. Axelrod, Microfilaments and actin-associated proteins at sites of membrane–substrate attachment within acetylcholine receptor clusters, *Exp. Cell Res. 182*, 583–596 (1989).
108. M. Nakache, H. E. Gaub, A. B. Screiber, and H. M. McConnell, Topological and modulated distribution of surface markers on endothelial cells, *Proc. Natl. Acad. Sci. U.S.A. 83*, 2874–2878 (1986).
109. D. Gingell, I. Todd, and J. Bailey, Topography of cell-glass apposition revealed by total internal reflection fluorescence of volume markers, *J. Cell Biol. 100*, 1334–1338 (1985).
110. D. Gingell, O. S. Heavens, and J. S. Mellor, General electromagnetic theory of internal reflection fluorescence: The quantitative basis for mapping cell-substratum topography, *J. Cell Sci. 87*, 677–693 (1987).
111. I. Todd, J. S. Mellor, and D. Gingell, Mapping cell–glass contacts of *Dictyostelium amoebae* by total internal reflection aqueous fluorescence overcomes a basic ambiguity of interference reflection microscopy, *J. Cell Sci. 89*, 107–114 (1988).
112. T. H. Watts, H. E. Gaub, and H. M. McConnell, T-cell-mediated association of peptide antigen and major histocompatibility complex protein detected by energy transfer in an evanescent wave-field, *Nature 320*, 176–179 (1986).
113. R. M. Sutherland, C. Dahne, J. F. Place, and A. S. Ringrose, Optical detection of antibody–antigen reactions at a glass–liquid interface, *Clin. Chem. 30*, 1533–1538 (1984).
114. E. Kalb, J. Engel, and L. K. Tamm, Binding proteins to specific target sites in membranes measured by total internal reflection fluorescence microscopy, *Biochemistry 29*, 1607–1613 (1990).
115. N. L. Thompson, T. P. Burghardt, and D. Axelrod, Measuring surface dynamics of biomolecules by total internal reflection with photobleaching recovery or correlation spectroscopy, *Biophys. J. 33*, 435–454 (1981).
116. G. Adam and M. Delbruck, Reduction of dimensionality in biological diffusion processes, in: *Structural Chemistry and Molecular Biology* (A. Rich and N. Davidson, eds.), pp. 198–215, W. H. Freeman, San Francisco (1968).
117. H. Berg and E. M. Purcell, Physics of chemoreception, *Biophys. J. 20*, 193–219 (1977).
118. R. D. Tilton, C. R. Robertson, and A. P. Gast, Lateral diffusion of bovine serum albumin adsorbed at the solid–liquid interface, *J. Colloid Interface Sci. 137*, 192–203 (1990).
119. R. D. Tilton, A. P. Gast, and C. R. Robertson, Surface diffusion of interacting proteins. Effect of concentration on the lateral mobility of adsorbed bovine serum albumin, *Biophys. J. 58*, 1321–1326 (1990).
120. K. H. Pearce, R. G. Hiskey, and N. L. Thompson, Binding kinetics of fluorescently labeled bovine prothrombin fragment 1 at planar model membranes measured by total internal reflection fluorescence microscopy, *Biophys. J. 59*, 622a (1991).
121. M. L. Pisarchik and N. L. Thompson, Surface binding kinetics of a monoclonal Fab fragment on supported phospholipid monolayers measured by total internal reflection/fluorescence photobleaching recovery, *Biophys. J. 59*, 350a (1991).
122. D. Axelrod, R. M. Fulbright, and E. H. Hellen, Adsorption kinetics on biological membranes: Measurement by total internal reflection fluorescence, in: *Applications of Fluorescence in the Biomedical Sciences* (D. L. Taylor, A. S. Waggoner, F. Lanni, R. F. Murphy, and R. Birge, eds.), pp. 461–467, Alan R. Liss, New York (1986).

123. R. M. Fulbright, Adsorption kinetics of insulin at erythrocyte membranes, Ph.D. thesis, University of Michigan (1991), manuscript submitted.
124. S.-F. Sui, T. Urumow, and E. Sackmann, Interaction of insulin receptors with lipid bilayers and specific and nonspecific binding of insulin to supported membranes, *Biochemistry 27*, 7463–7469 (1988).
125. E. H. Hellen and D. Axelrod, Kinetics of epidermal growth factor/receptor binding on cells measured by total internal reflection/fluorescence recovery after photobleaching, *J. Fluor. 1*, 113–128 (1991).
126. T. Hirschfeld, M. J. Block, and W. Mueller, Virometer: An optical instrument for visual observation, measurement and classification of free viruses, *J. Histochem. Cytochem. 25*, 719–723 (1977).
127. N. L. Thompson and D. Axelrod, Immunoglobulin surface-binding kinetics studied by total internal reflection with fluorescence correlation spectroscopy, *Biophys. J. 43*, 103–114 (1983).
128. N. L. Thompson, Surface binding rates of nonfluorescent molecules may be obtained by total internal reflection with fluorescence correlation spectroscopy, *Biophys. J. 38*, 327–329 (1982).
129. D. Gingell and I. Todd, Interference reflection microscopy. A quantitative theory for image interpretation and its application to cell-substratum separation measurement, *Biophys. J. 26*, 507–526 (1979).